Cell

Article

Elicitation of broadly protective sarbecovirus immunity by receptor-binding domain nanoparticle vaccines

Graphical abstract

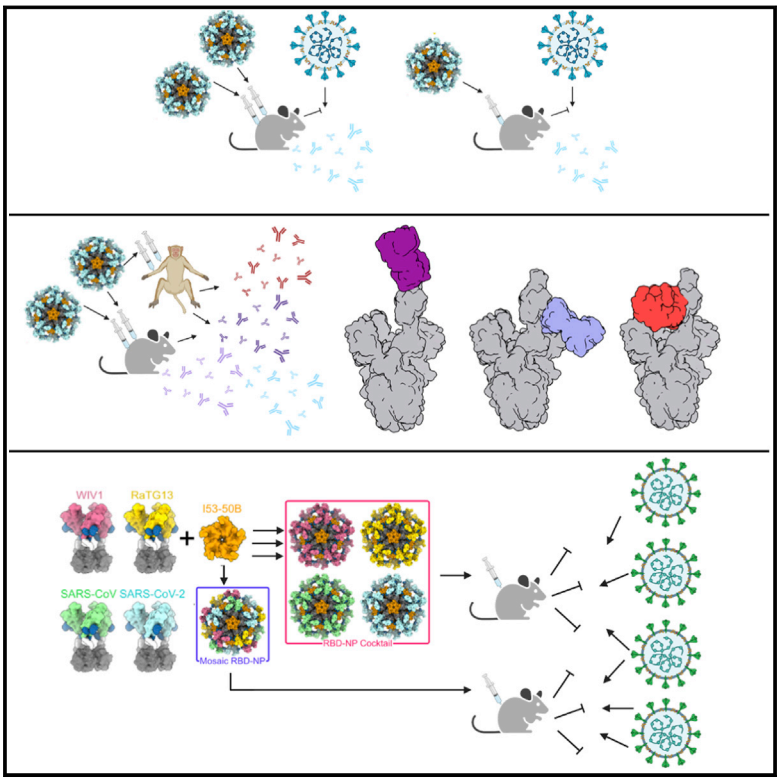

Authors

Alexandra C. Walls, Marcos C. Miranda, Alexandra Schäfer, ..., Ralph S. Baric, Neil P. King, David Veesler

Correspondence

neil@ipd.uw.edu (N.P.K.), dveesler@uw.edu (D.V.)

In brief

A clinical stage multivalent SARS-CoV-2 spike receptor-binding domain nanoparticle (RBD-NP) vaccine is protective in mice after a single immunization and elicits strong antibody responses across circulating mutants and some sarbecoviruses. Multivalent sarbecovirus RBD-NP vaccines elicit heterotypic protection against sarbecoviruses.

Highlights

- RBD-NP enables dose-sparing and protects mice after only one dose
- RBD-NP elicits diverse polyclonal antibody responses in non-human primates
- RBD-NP and HexaPro confer similar resilience to antigenic drift
- Mosaic and cocktail RBD-NPs protect against heterotypic SARS-CoV challenge

Walls et al., 2021, Cell *184*, 5432–5447
October 14, 2021
https://doi.org/10.1016/j.cell.2021.09.015

CellPress

CellPress

Cell

Article

Elicitation of broadly protective sarbecovirus immunity by receptor-binding domain nanoparticle vaccines

Alexandra C. Walls,[1] Marcos C. Miranda,[1,2] Alexandra Schäfer,[3] Minh N. Pham,[1,2] Allison Greaney,[4,5] Prabhu S. Arunachalam,[6] Mary-Jane Navarro,[1] M. Alejandra Tortorici,[1,7] Kenneth Rogers,[8] Megan A. O'Connor,[9,10] Lisa Shirreff,[8] Douglas E. Ferrell,[8] John Bowen,[1] Natalie Brunette,[1,2] Elizabeth Kepl,[1,2] Samantha K. Zepeda,[1] Tyler Starr,[4] Ching-Lin Hsieh,[11] Brooke Fiala,[1,2] Samuel Wrenn,[1,2] Deleah Pettie,[1,2] Claire Sydeman,[1,2] Kaitlin R. Sprouse,[1] Max Johnson,[1,2] Alyssa Blackstone,[1,2] Rashmi Ravichandran,[1,2] Cassandra Ogohara,[1,2] Lauren Carter,[1,2] Sasha W. Tilles,[12] Rino Rappuoli,[13] Sarah R. Leist,[3] David R. Martinez,[3] Matthew Clark,[14] Roland Tisch,[15] Derek T. O'Hagan,[16] Robbert Van Der Most,[17] Wesley C. Van Voorhis,[12] Davide Corti,[18] Jason S. McLellan,[11] Harry Kleanthous,[19] Timothy P. Sheahan,[3] Kelly D. Smith,[20] Deborah H. Fuller,[9,10] Francois Villinger,[8] Jesse Bloom,[4,5] Bali Pulendran,[6] Ralph S. Baric,[3] Neil P. King,[1,2,*] and David Veesler[1,21,*]

[1]Department of Biochemistry, University of Washington, Seattle, WA 98195, USA
[2]Institute for Protein Design, University of Washington, Seattle, WA 98195, USA
[3]Department of Epidemiology, University of North Carolina at Chapel Hill, Chapel Hill, NC 27514, USA
[4]Basic Sciences and Computational Biology, Fred Hutchinson Cancer Research Center, Seattle, WA 98109, USA
[5]Department of Genome Sciences, University of Washington, Seattle, WA 98109, USA
[6]Institute for Immunity, Transplantation and Infection, Stanford University School of Medicine, Stanford University, Stanford, CA, USA
[7]Institut Pasteur and CNRS UMR 3569, Unite de Virologie Structurale, Paris, France
[8]New Iberia Research Center and Department of Biology, University of Louisiana at Lafayette, New Iberia, LA 70560, USA
[9]Washington National Primate Research Center, Seattle, WA 98121, USA
[10]Department of Microbiology, University of Washington, Seattle, WA 98195, USA
[11]Department of Molecular Biosciences, The University of Texas at Austin, Austin, TX 78712, USA
[12]Division of Allergy and Infectious Diseases, Department of Medicine, University of Washington School of Medicine, Seattle, WA 98195, USA
[13]GSK, Siena, Italy
[14]Department of Microbiology and Immunology, University of North Carolina at Chapel Hill, Chapel Hill, NC 27514, USA
[15]Lineberger Comprehensive Cancer Center, University of North Carolina at Chapel Hill, Chapel Hill, NC 27514, USA
[16]GSK, Rockville, MD, USA
[17]GSK, Rixensart, Belgium
[18]Humabs Biomed SA, a subsidiary of Vir Biotechnology, 6500 Bellinzona, Switzerland
[19]Bill & Melinda Gates Foundation, Seattle, WA 98109, USA
[20]UW Medicine Department of Laboratory Medicine and Pathology, Seattle, WA 98195, USA
[21]Lead contact
*Correspondence: neil@ipd.uw.edu (N.P.K.), dveesler@uw.edu (D.V.)
https://doi.org/10.1016/j.cell.2021.09.015

SUMMARY

Understanding vaccine-elicited protection against SARS-CoV-2 variants and other sarbecoviruses is key for guiding public health policies. We show that a clinical stage multivalent SARS-CoV-2 spike receptor-binding domain nanoparticle (RBD-NP) vaccine protects mice from SARS-CoV-2 challenge after a single immunization, indicating a potential dose-sparing strategy. We benchmarked serum neutralizing activity elicited by RBD-NPs in non-human primates against a lead prefusion-stabilized SARS-CoV-2 spike (HexaPro) using a panel of circulating mutants. Polyclonal antibodies elicited by both vaccines are similarly resilient to many RBD residue substitutions tested, although mutations at and surrounding position 484 have negative consequences for neutralization. Mosaic and cocktail nanoparticle immunogens displaying multiple sarbecovirus RBDs elicit broad neutralizing activity in mice and protect mice against SARS-CoV challenge even in the absence of SARS-CoV RBD in the vaccine. This study provides proof of principle that multivalent sarbecovirus RBD-NPs induce heterotypic protection and motivates advancing such broadly protective sarbecovirus vaccines to the clinic.

INTRODUCTION

The emergence of SARS-CoV-2 in late 2019 resulted in the COVID-19 pandemic that brought the world to a standstill. Moreover, the recurrent spillovers of coronaviruses in humans along with detection of SARS-CoV-2-, SARS-CoV-, and MERS-CoV-related coronaviruses in bats suggest that future zoonotic transmission events may continue to occur (Menachery et al., 2015, 2016; Zhou et al., 2020a). SARS-CoV-2 infects host cells through the attachment of the viral transmembrane spike (S) glycoprotein to angiotensin-converting enzyme 2 (ACE2), followed by fusion of the viral and host membranes (Hoffmann et al., 2020; Lan et al., 2020; Letko et al., 2020; Shang et al., 2020; Walls et al., 2020a; Wang et al., 2020; Wrapp et al., 2020; Yan et al., 2020; Zhou et al., 2020b). The SARS-CoV-2 S protein is the primary target of neutralizing antibodies (Abs), and the immunodominant receptor-binding domain (RBD) accounts for more than 90% of the neutralizing activity in COVID-19 convalescent sera and vaccinated individuals (Greaney et al., 2021a, 2021b; Piccoli et al., 2020). Numerous monoclonal Abs (mAbs) recognizing distinct antigenic sites on the RBD were isolated and shown to neutralize viral entry and protect small animals and non-human primates (NHPs) from SARS-CoV-2 challenge (Barnes et al., 2020; Baum et al., 2020a; Brouwer et al., 2020; Piccoli et al., 2020; Pinto et al., 2020; Rogers et al., 2020; Starr et al., 2021; Tortorici et al., 2020; Wec et al., 2020; Zost et al., 2020). As a result, SARS-CoV-2 S is the focus of nucleic acid, vectored, and protein subunit vaccines currently being developed and deployed (Corbett et al., 2020a, 2020b; Jackson et al., 2020; Mercado et al., 2020; Polack et al., 2020; Tostanoski et al., 2020; Yu et al., 2020).

Worldwide sequencing of SARS-CoV-2 clinical isolates has led to the identification of numerous mutations in the >1,500,000 genome sequences available to date (https://www.gisaid.org/). The SARS-CoV-2 S D614G mutation has become globally dominant and is associated with enhanced viral transmission and replication but does not significantly affect Ab-mediated neutralization (Hou et al., 2020; Korber et al., 2020; Plante et al., 2020; Yurkovetskiy et al., 2020). Conversely, some mutations found in circulating SARS-CoV-2 isolates were shown to promote escape from mAbs and to reduce neutralization by immune sera (Baum et al., 2020b; Collier et al., 2021; Li et al., 2020; McCallum et al., 2021a, 2021b; Wang et al., 2021a; Weisblum et al., 2020; Wibmer et al., 2021). As a result, formulation of mAb cocktails or the use of mAbs targeting conserved epitopes and neutralizing a broader spectrum of circulating SARS-CoV-2 variants emerged as a promising strategy to overcome this issue (Baum et al., 2020b; Cathcart et al., 2021; Dong et al., 2021; Greaney et al., 2020; Jette et al., 2021; Martinez et al., 2021a; Pinto et al., 2020; Tortorici et al., 2020, 2021). The recent emergence of several variants and variants of concern (VOCs) with numerous S mutations is especially worrisome, including B.1.1.7 (alpha), B.1.351 (beta), B.1.427/B.1.429 (epsilon), P.1 (gamma), and B.1.617.2 (delta) that originated in the UK, South Africa, the USA, Brazil, and India, respectively (Davies et al., 2020; Deng et al., 2021; Faria et al., 2021; McCallum et al., 2021b; Tegally et al., 2020). Some of these mutations lead to significant reductions in the neutralization potency of N-terminal domain (NTD)- and RBD-specific mAbs, convalescent sera, and Pfizer/BioNTech BNT162b2- or Moderna mRNA-1273-elicited sera (Collier et al., 2021; McCallum et al., 2021a, 2021b; Wang et al., 2021a).

We recently described a multivalent subunit vaccine displaying the SARS-CoV-2 RBD nanoparticle (RBD-NP) in a highly immunogenic array using a computationally designed self-assembling protein nanoparticle (Bale et al., 2016; Walls et al., 2020b). Vaccination with RBD-NP resulted in 10-fold higher neutralizing Ab titers in mice than the prefusion-stabilized S2P trimer (which is used in most current vaccines) despite a 5-fold lower dose and protected mice against mouse-adapted SARS-CoV-2 (SARS-CoV-2-MA) challenge (Dinnon et al., 2020; Walls et al., 2020b). We demonstrated that the RBD-NP vaccine elicited robust neutralizing Ab and CD4 T cell responses in NHPs when formulated with several clinic-ready adjuvants and conferred protection against SARS-CoV-2 infection in the nose, pharynges, and bronchioles (Arunachalam et al., 2021). The RBD-NP vaccine is currently being evaluated in two phase I/II clinical trials (ClinicalTrials.gov: NCT04742738 and NCT04750343) and recently received funding from the coalition for epidemic preparedness innovations for phase III clinical trials.

Although the S fusion machinery (S_2 subunit) has higher sequence conservation than the RBD (Pinto et al., 2021; Sauer et al., 2021; Tortorici and Veesler, 2019; Walls et al., 2016, 2020a), the breadth of neutralization and protection provided by RBD-based vaccines remains unknown. The isolation of RBD-specific cross-reactive mAbs neutralizing SARS-CoV-2 and SARS-CoV suggests that RBD-based vaccines could, in principle, elicit Abs that neutralize distantly related sarbecoviruses, which have future pandemic potential (Cathcart et al., 2021; Jette et al., 2021; Martinez et al., 2021a; Pinto et al., 2020; Rappazzo et al., 2021; Starr et al., 2021; Tortorici et al., 2021; Wec et al., 2020). RBD-based vaccines are also unaffected by S mutations outside of the RBD, especially in the highly variable NTD that is heavily mutated in many VOCs (Andreano et al., 2020; Avanzato et al., 2020; Choi et al., 2020; Collier et al., 2021; Wang et al., 2021a; McCallum et al., 2021a, 2021b; McCarthy et al., 2021). Here, we explored dose-sparing strategies for the RBD-NP vaccine and evaluated the impact of genetic diversity among SARS-CoV-2 clinical isolates and sarbecoviruses on vaccine-elicited Abs. We further designed mosaic and cocktail sarbecovirus RBD-NPs that elicit broad and protective Ab responses against heterologous sarbecovirus challenge, which could represent the next generation of pan-sarbecovirus vaccines.

RESULTS

Dose-sparing RBD-NP vaccination protects mice against SARS-CoV-2 challenge

Considering the unprecedented need for rapid global distribution of SARS-CoV-2 vaccines, we investigated the ability of RBD-NP to induce neutralizing and protective Ab titers at lower doses than previously evaluated. Specifically, we set out to test whether vaccine-elicited neutralizing Ab titers are altered by lowering the immunogen dose 10-fold (two 0.1 μg immunizations, RBD antigen dose) or reducing the number of doses

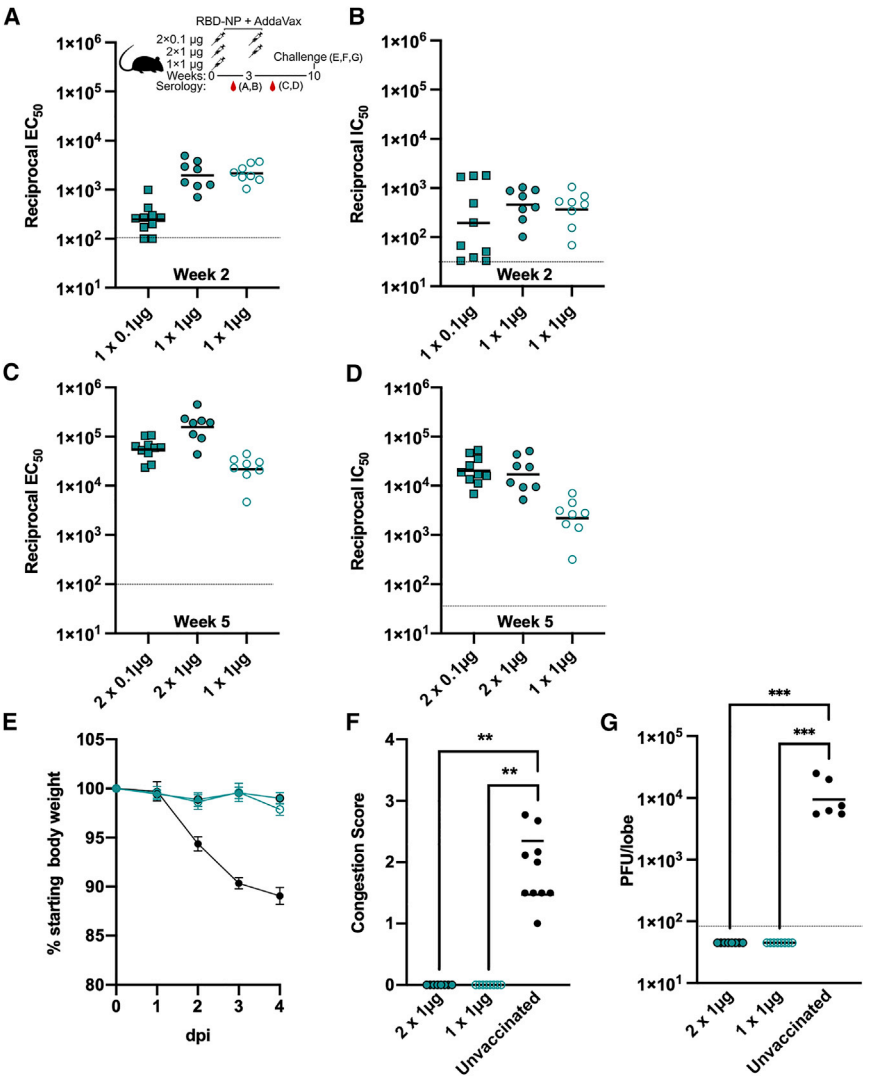

Figure 1. A single immunization with RBD-NP protects BALB/c cByJ mice from SARS-CoV-2 MA10 challenge

(A and C) S2P-binding Abs were measured 2 (A) or 5 (C) weeks post-prime; teal squares: 2 doses of 0.1 μg (n = 10); filled teal circles: 2 doses of 1 μg (n = 8); open teal circles: one dose of 1 μg (n = 8) with a limit of detection (LOD) of 1×10^2.

(B and D) Serum neutralizing Ab titers at 2 (B) or 5 (D) weeks post-prime determined using an MLV pseudotyping system with an LOD of 3.3×10^1.

(E) Weight loss following SARS-CoV-2 MA10 challenge up to 4 days post infection (n = 8 vaccinated; n = 6 naive mice shown as black filled circles).

(F) Congestion score following SARS-CoV-2 MA10 challenge with a score of 0 indicating unchanged lung color and 4 indicating a darkened and diseased lung.

(G) Viral titers in the mice lungs (expressed in plaque forming units [PFUs] per lobe) following challenge with an LOD of 9×10^1. Statistical significance was determined by Kruskal-Wallis test and shown only when significant. $^{**}p < 0.01$. LODs are shown as gray horizontal dotted lines.

Raw data curves shown in Data S1.

(a single 1 μg immunization, RBD antigen dose) compared to our initial work (Walls et al., 2020b). To test this, BALB/c cByJ mice were immunized intramuscularly at week 0 with either 0.1 μg (ten mice) or 1 μg (two groups of eight mice or sixteen mice total) of AddaVax-adjuvanted RBD-NP. Two weeks post-prime, serum binding and neutralizing Ab titers were roughly comparable for the two vaccine doses (neutralization geometric mean titer [GMT] ~2–4 × 10^2) measured using a mouse leukemia virus (MLV) pseudotyping system (Millet and Whittaker, 2016; Walls et al., 2020a) (Figures 1A and 1B; Data S1). Three weeks post prime, we boosted the mice that were immunized with 0.1 μg of the vaccine and eight of the sixteen mice immunized with 1 μg of the vaccine with the same respective dose. Two weeks post-boost, serum binding and neutralizing Ab titers were comparable for the 0.1 μg and 1 μg groups (neutralization GMT ~2 × 10^4) (Figures 1C and 1D; Data S1), suggesting that a 10-fold reduction in the RBD-NP dose does not affect serum neutralizing responses. Furthermore, we observed that the magnitude of binding and neutralizing Ab titers increased over time for the mice that received a single immunization (neutralization GMT 2 × 10^3). These results suggest that lowering the vaccine dose or reducing the number of immunizations represent possible dose-sparing strategies that did not compromise elicitation of high levels of neutralizing Ab titers using RBD-NPs.

To further evaluate vaccine efficacy, eight mice that received one dose and eight mice that received two doses of the 1-μg RBD-NP vaccine along with six unvaccinated mice were challenged ten weeks post-prime with 10^5 plaque-forming units (PFUs) of mouse-adapted SARS-CoV-2 MA10 (Leist et al., 2020). The SARS-CoV-2 MA10 model causes weight loss and lung pathology when 10^5 PFUs (the highest titer tested [Leist et al., 2020]) are used in young BALB/c mice. The mice were followed for four days to assess protection from disease. All mice in the RBD-NP-vaccinated groups were protected from weight loss throughout the duration of the experiment regardless of the number of doses, whereas control mice lost ~10% of their weight by day four (Figure 1E). Analysis of lung pathology and viral titers in lung tissues indicated that the vaccinated mice were not affected by SARS-CoV-2 MA10 challenge, whereas the control mice showed lung discoloration four days post-infection and a high viral load (~1 × 10^4 PFUs) (Figures 1F and 1G). These results indicate that one or two immunizations with 1 μg RBD-NPs results in protection against SARS-CoV-2 MA10-induced disease. Furthermore, mice vaccinated twice with a 10-fold lower dose of RBD-antigen (0.1 μg) had higher

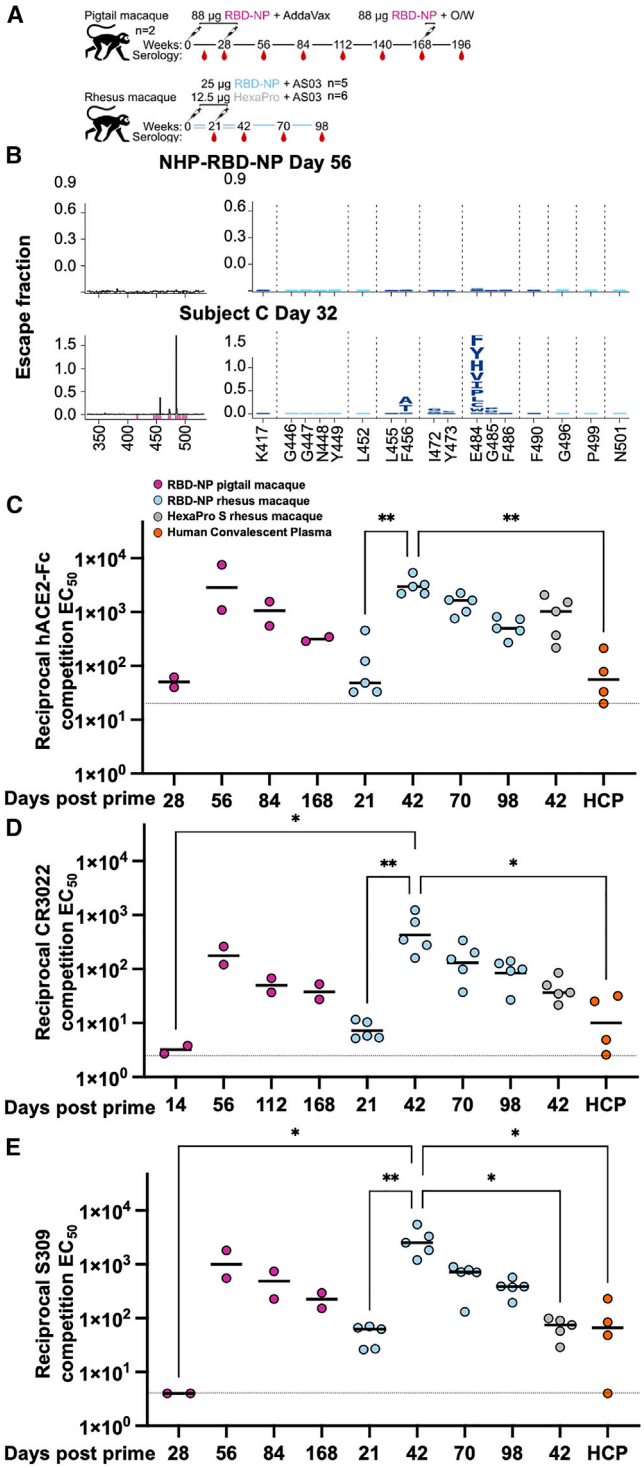

Figure 2. RBD-NP vaccination elicits high titers of Abs targeting diverse RBD antigenic sites in NHPs

(A) NHP study designs.

(B) Effect of RBD mutations on polyclonal Ab binding measured by DMS analysis of serum obtained 8 weeks post-prime from an immunized pigtail macaque (n = 1) compared to a previously reported DMS measurement from a representative COVID-19 HCP sample (reproduced here for comparison; Greaney et al., 2021b). The line plots on the left show the summed effect of all mutations at a site in the RBD on serum or plasma binding, with RBD residues on the x axis and Ab escape on the y axis (Table S1). Due to the use of sample-specific FACS gates (Figure S1), the y axes are scaled independently. Sites in the logo plots are colored dark blue if located in the receptor-binding ridge or cyan if located in the RBD 443–450 loop. Larger values indicate more Ab escape.

(C–E) Competition ELISA between 0.2-nM hACE2-Fc (LOD of 2 × 10^{1}) (C), 2-nM CR3022 mAb (LOD of 2 × 10^{0}) (D), or 0.01-nM S309 mAb (LOD of 4 × 10^{0}) (E), and RBD-NP-elicited sera in pigtail macaques (n = 2), RBD-NP-elicited sera in rhesus macaques (n = 5), or HexaPro S-elicited sera in rhesus macaques (n = 5) at various time points following vaccination, benchmarked against HCP (n = 4) (Table S2). Each plot shows the magnitude of inhibition of hACE2/mAb binding to immobilized SARS-CoV-2 S2P, expressed as reciprocal serum dilution blocking 50% of the maximum binding response. Statistical significance was determined by Kruskal-Wallis test and shown only when significant. **p < 0.01. LODs are shown as gray horizontal dotted lines.

Raw data curves shown in Data S1.

serum neutralizing Ab titers than mice receiving a single 1-µg dose, suggesting that they would likely also be protected since neutralizing Ab titers are a correlate of protection against SARS-CoV-2 (Arunachalam et al., 2021; McMahan et al., 2021). These data suggest that multiple RBD-NP dose-sparing regimens may be possible.

RBD-NP vaccination induces Abs targeting diverse antigenic sites in NHPs

To characterize the epitopes targeted by RBD-NP-elicited polyclonal Abs, we used deep mutational scanning (DMS) with sera obtained 56 days post-prime from one of two pigtail macaques immunized at days 0 and 28 with a dose of AddaVax-adjuvanted RBD-NP containing 88 µg of the SARS-CoV-2 RBD (with a linker of twelve glycine/serine (GS) residues between the RBD and the NP) (Walls et al., 2020b) (Figures 2A and 2B). These experiments rely on yeast surface display of RBD libraries covering nearly all possible amino acid mutations coupled with fluorescence-activated cell sorting (FACS) to identify RBD mutants with attenuated Ab binding compared to the wild-type (Wuhan-Hu-1) SARS-CoV-2 RBD (Greaney et al., 2020; Starr et al., 2020a). No single mutation had more than a marginal effect on serum Ab (IgG/IgM/IgA) binding, indicating broad targeting of distinct RBD epitopes, whereas several previously described COVID-19 human convalescent plasmas (HCPs) analyzed by DMS displayed greater sensitivity to individual mutations and are shown for comparison (Greaney et al., 2021b) (Figures 2B and S1; Table S1). These results show that RBD-NP vaccination elicits highly diverse polyclonal Ab responses that target multiple distinct antigenic sites and are more resilient to escape mutations reducing polyclonal Ab binding than HCP (Barnes et al., 2020; Greaney et al., 2021b; Piccoli et al., 2020; Starr et al., 2021).

To measure the magnitude of vaccine-elicited Abs against distinct RBD antigenic sites, we used quantitative competition ELISAs with human ACE2-Fc (hACE2-Fc), which binds to the receptor-binding motif (RBM) corresponding to antigenic sites Ia and Ib, as well as with structurally characterized mAbs recognizing antigenic sites II (CR3022) and IV (S309) (Huo et al., 2020; Piccoli et al., 2020; Pinto et al., 2020; Yuan et al., 2020) (Figures 2C–2E; Data S1). These experiments

used sera from the aforementioned pigtail macaques (RBD GMT EC_{50} 5×10^4) followed for 168 days and sera from 5 rhesus macaques immunized twice on days 0 and 21 with AS03-adjuvanted RBD-NPs containing 25 μg of the SARS-CoV-2 RBD (with a 16-GS linker between the RBD and the NP; RBD GMT EC_{50} 1×10^4) and followed for 98 days (Arunachalam et al., 2021; Walls et al., 2020b; Figures 2A and S2A). These two sets of RBD-NP sera were compared to sera from 5 rhesus macaques immunized twice on days 0 and 21 with 12.5 μg of AS03-adjuvanted prefusion-stabilized HexaPro S trimer (RBD EC_{50} 1×10^4) and followed for 42 days (Arunachalam et al., 2021; Hsieh et al., 2020), as well as a panel of COVID-19 HCP (Table S2) (RBD EC_{50} 2×10^4) (Figures 2A and S2A). All NHP sera post boost had high titers of Abs targeting sites Ia and Ib in the immunodominant RBM (day 42 hACE2 competition RBD-NP GMT 3×10^3 and HexaPro GMT 7×10^2) (Figure 2C; Data S1), a correlate of neutralization potency (Piccoli et al., 2020), in agreement with the potent immunogenicity and protective efficacy of RBD-NP and HexaPro S in NHPs (Arunachalam et al., 2021). We also observed strong Ab responses against antigenic sites II (RBD-NP day 42 GMT 4×10^2 and HexaPro GMT 4×10^1) with CR3022 competition and IV (RBD-NP day 42 GMT 2.5×10^3 and HexaPro GMT 6.5×10^1) (Figures 2D and 2E; Data S1), which comprise conserved sarbecovirus epitopes recognized by broadly neutralizing sarbecovirus mAbs such as S2X259 (site II) and S309 (site IV) (Piccoli et al., 2020; Pinto et al., 2020; Tortorici et al., 2021). Ab responses were durable against all 3 antigenic sites regardless of dose or adjuvant, with a decrease of competition titers by roughly half an order to one order of magnitude 168 days (pigtail macaque) or 98 days (rhesus macaque) post-prime. RBD-NP elicited much higher peak binding titers toward all RBD antigenic sites evaluated compared to HexaPro S and HCP, showcasing the potency, durability, and multi-specificity of Ab responses induced by multivalent display of the RBD, possibly as a result of enhanced accessibility of the antigen.

RBD-NP vaccine elicits potent neutralizing Ab responses in NHPs against a panel of SARS-CoV-2 S variants

To assess the neutralization breadth of RBD-NP- and HexaPro S-elicited Abs in NHPs at peak titer (42 days post-prime), we evaluated serum neutralizing activity against a panel of pseudotyped viruses comprising wild-type (D614G) SARS-CoV-2 S and twelve single-residue SARS-CoV-2 RBD mutants detected in clinical isolates (N439K, L452R, Y453F, L455F, S477N, E484A/K/Q, F486L, S494P, N501Y, and G504D) as well as the B.1.1.7 (H69-V70 deletion, Y144 deletion, N501Y, A570D, D614G, P681H, T716I, S982A, D1118H); B.1.1.7 + E484K (H69-V70 deletion, Y144 deletion, E484K, N501Y, A570D, D614G, P681H, T716I, S982A, D1118H); B.1.351 (L18F, D80A, D215G, L242-L244 deletion, R246I, K417N, E484K, N501Y, D614G, A701V); and P.1 (L18F, T20N, P26S, D138Y, R190S, K417T, E484K, N501Y, D614G, H655Y, T1027I). Several single-residue RBD mutations did not affect neutralizing titers compared to wild-type D614G SARS-CoV-2 S, for which GMTs of 1.8×10^3 and 2.4×10^3 were determined with RBD-NP- and HexaPro S-elicited sera, respectively, using a vesicular stomatitis virus (VSV) pseudotyped virus (Figure 3A; Data S1). For example, the N439K- (GMT 2.5×10^3 for RBD-NP and 2.7×10^3 for HexaPro S) and mink-associated Y453F (GMT 4×10^3 for RBD-NP and 5×10^3 for HexaPro S) mutation did not dampen the neutralization potency of either RBD-NP- or HexaPro S-elicited sera (Figure 3A; Data S1). However, the N501Y substitution (present in the B.1.1.7, P.1, and B.1.351 lineages) reduced the neutralization potency of RBD-NP- (GMT 5×10^2) and HexaPro S (GMT 8×10^2)-elicited sera 3-to-4-fold and the L452R mutation (present in the B.1.427/B.1.429, B.1.617.1, and B.1.617.22 variant) led to a 3.4-to-4.4-fold drop in neutralization potency (GMT 4×10^2 for RBD-NP and 7×10^2 for HexaPro S). These substitutions have been associated with the loss of binding and neutralization for vaccine-elicited Abs and mAbs (Collier et al., 2021; McCallum et al., 2021b; Wang et al., 2021b; Thomson et al., 2021; Wang et al., 2021c). The E484A mutation reduced serum neutralization activity up to 2-fold (GMT $1.1x10^3$ for RBD-NP and $1.1x10^3$ for HexaPro S) whereas E484K, present in B.1.351 and P1 (GMT 2×10^2 for RBD-NP and 2×10^2 for HexaPro S), and E484Q, found in B.1.617.1 (GMT 5×10^2 for RBD-NP and 3.6×10^2 for HexaPro S), decreased it 9-fold (E484K) and 4-fold (E484Q) for RBD-NP and 12-fold (484K) and 7-fold (484Q) for HexaPro S compared to D614G SARS-CoV-2 S. These experiments suggest that a substantial fraction of the neutralizing activity elicited by both RBD-NP and HexaPro S is focused on the RBM, especially near position 484, as further supported by the ~5-fold decrease in neutralization resulting from the F486L (GMT 3.7×10^2 for RBD-NP and 5×10^2 for HexaPro S) substitution.

To understand the impact of the full constellation of mutations present in the S proteins of the aforementioned VOCs, we evaluated RBD-NP- and HexaPro S-elicited serum neutralizing activity against corresponding HIV and VSV pseudotyped variants (D614G GMT RBD-NP HIV 5×10^3 and VSV RBD-NP 6×10^2, respectively, and D614G GMT HexaPro S HIV 3.5×10^3 and VSV 1.2×10^3) (Figures 3B and 3C). Although we did not observe major reductions in neutralization titers (up to to 2-fold) toward the B.1.1.7 VOC (GMT RBD-NP HIV 2.5×10^3, VSV 4.7×10^2 and HexaPro S HIV 1.8×10^3, VSV 8.8×10^2) (Figures 3B and 3C), addition of the E484K mutation to the B.1.1.7 background reduced neutralization 4-to-6-fold for RBD-NP- (GMT HIV 8.8×10^2) and HexaPro S-elicited sera (GMT HIV 8.6×10^2), confirming the importance of the 484 position (Figure 3B). Neutralization of B.1.351 was 10-fold lower using HIV pseudovirus (GMT RBD-NP 5×10^2 and HexaPro S $3.6x10^2$) (Figure 3B) and ~3-fold lower using VSV pseudovirus (GMT RBD-NP 2×10^2 and HexaPro S $4x10^2$) (Figure 3C) for both RBD-NP- and HexaPro-elicited sera, in agreement with authentic virus neutralization data (Arunachalam et al., 2021). Interestingly, RBD-specific binding Ab titers did not differ significantly between the B.1.351 RBD (GMT RBD-NP 6.5×10^3 and HexaPro S 3×10^3) and Wuhan-Hu-1 RBD (GMT RBD-NP 1.4×10^4 and HexaPro S 1.7×10^4) (Figure S2A), indicating that neutralizing activity is accounted for by a portion of total binding Abs. Reductions in neutralizing Ab titers were also observed against P.1 S VSV pseudoviruses, with a 6-fold drop for RBD-NP (GMT 1×10^2) and 8-fold dampening for HexaPro S (GMT 1.5×10^2) (Figure 3C). Furthermore, we observed a 10-fold reduction in plasma

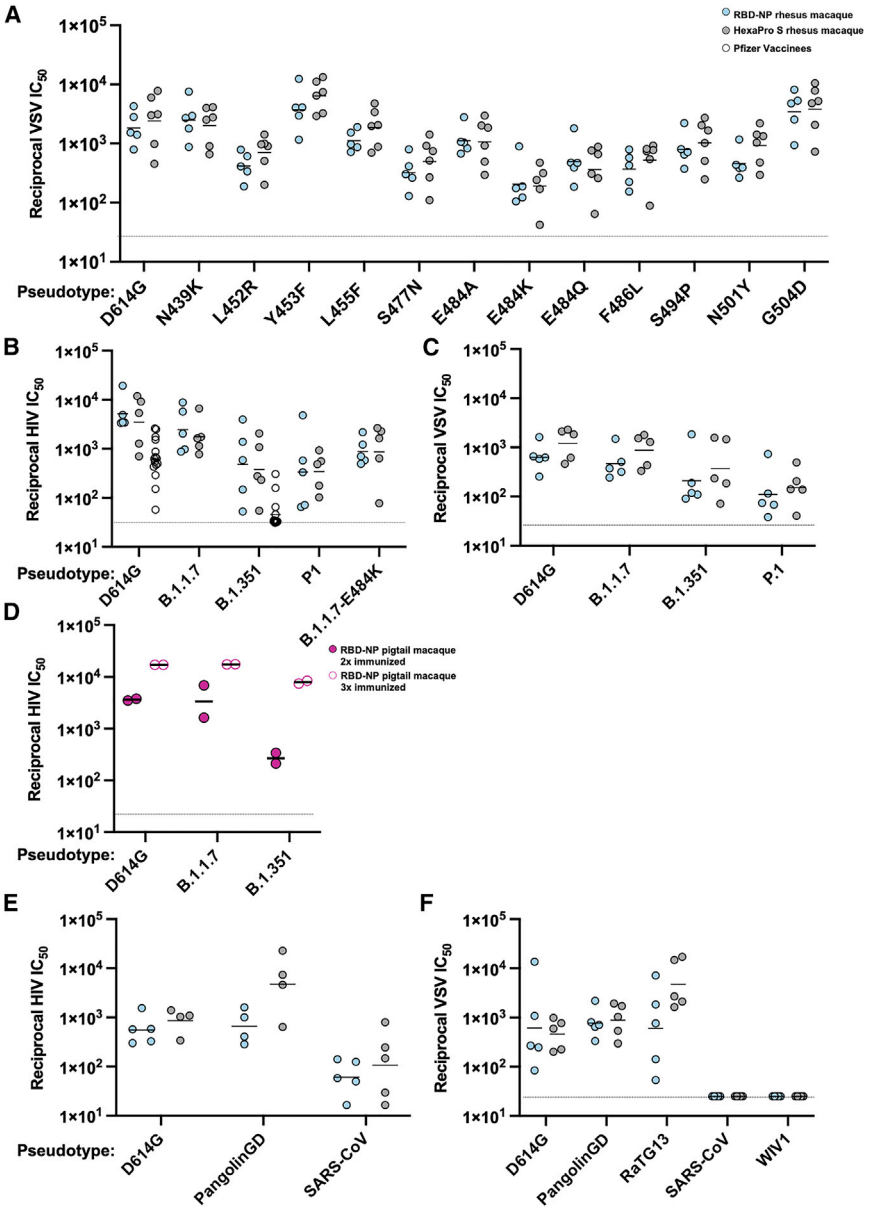

Figure 3. RBD-NP and HexaPro S elicit Abs with similar neutralization breadth toward SARS-CoV-2 variants

(A) Neutralizing Ab titers against wild-type (D614G) SARS-CoV-2 S and RBD point mutants determined using RBD-NP-elicited sera in rhesus macaques (blue, n = 5) and HexaPro S-elicited sera in rhesus macaques (gray, n = 6) with an VSV pseudotyping system with an LOD of 3.3 × 10^1. Neutralization performed once.

(B) Neutralizing Ab titers against HIV pseudotyped viruses harboring wild-type (D614G) SARS-CoV-2 S, B.1.1.7 S, B.1.1.7-E484K S, B.1.351 S, or P.1 S, determined using RBD-NP-elicited sera in rhesus macaques (blue), HexaPro S-elicited sera in rhesus macaques (gray), or plasma from individuals who received two doses of Pfizer mRNA vaccine (open circles) with an LOD of 3.3 × 10^1. Neutralization performed twice and a representative shown.

(C) Neutralizing Ab titers against VSV pseudotyped viruses harboring wild-type (D614G) SARS-CoV-2 S, B.1.1.7 S, B.1.351 S, or P.1 S, determined using RBD-NP-elicited sera in rhesus macaques (blue) or HexaPro S-elicited sera in rhesus macaques (gray) with an LOD of 2.5 × 10^1. Neutralization performed twice and a representative shown.

(D) Neutralizing Ab titers against D614G SARS-CoV-2 S, B.1.1.7, and B.1.351 S HIV pseudoviruses in pigtail macaque sera collected 28 days after a second (filled symbols, n = 2) or third (open symbols, n = 2) immunization with 88-μg RBD-NP (RBD antigen dose) with an LOD of 1 × 10^2. Neutralization performed twice and a representative shown.

(E) Neutralizing Ab titers against HIV pseudotyped viruses harboring wild-type (D614G) SARS-CoV-2 S, Pangolin-GD S, or SARS-CoV S, determined using RBD-NP-elicited sera in in rhesus macaques (blue) or HexaPro S-elicited sera in rhesus macaques (gray) with an LOD of 1 × 10^1. Neutralization performed twice and a representative shown.

(F) Neutralizing Ab titers against VSV pseudotyped viruses harboring wild-type (D614G) SARS-CoV-2 S, Pangolin-GD S, RaTG13 S, SARS-CoV S, or WIV1 S determined using SARS-CoV-2 RBD-NP-elicited sera in rhesus macaques (blue) or HexaPro S-elicited sera in rhesus macaques (gray) with an LOD of 2.5 × 10^1. Neutralization performed twice and a representative shown. Statistical significance was determined by Kruskal-Wallis test and shown in Table S3. LODs are shown as gray horizontal dotted lines. Raw data curves shown in Data S1 and GMTs in Table S4. The various pseudovirus backbones were benchmarked against NIBSC standard and are shown in Table S5.

neutralizing potency for individuals who received two doses of the Pfizer-BioNTech BNT162b2 mRNA vaccine against B.1.351 S pseudotyped virus (GMT 6 × 10^1) relative to the wild-type (D614G) SARS-CoV-2 S (GMT 6 × 10^2) pseudotyped virus (Figure 3B; Data S1). These findings show that, as is the case for many convalescent individuals (Greaney et al., 2021b; Liu et al., 2021; Piccoli et al., 2020), an important fraction of vaccine-elicited neutralizing Abs in NHPs and humans is focused on the RBM (specifically around position 484), independently of the immunogen (RBD-NP, HexaPro S, or 2P-stabilized S [Pallesen et al., 2017]) or the vaccine modality (protein subunit or mRNA). However, we note that neutralization assays may underestimate the contribution of NTD-specific or non-RBM RBD-targeted neutralizing Abs (Lempp et al., 2021; McCallum et al., 2021a; Suryadevara et al., 2021), and protection from challenge will be the ultimate readout.

To further investigate the relationships between neutralizing Ab titers and emerging SARS-CoV-2 variants, we immunized the two pigtail macaques a third time with RBD-NP, formulated with an oil-in-water (O/W) emulsion-based adjuvant, 168 days after the primary immunization (Figure 2A). This boost induced potent serum neutralizing activity against wild-type (D614G)

SARS-CoV-2 (GMT 2 × 10^4) (Figure 3D) as well as the B.1.1.7 (GMT 2 × 10^4) and B.1.351 (GMT 8 × 10^3) VOC pseudoviruses, suggesting that an overall increase in neutralizing Ab titers may be a suitable strategy to cope with emerging variants. These results are consistent with recent studies demonstrating that boosting COVID-19 convalescent individuals with a single mRNA vaccination elicited high (neutralizing) Ab titers, including against the B.1.351 variant (Abu Jabal et al., 2021; Krammer et al., 2021; Stamatatos et al., 2021), and suggest that a third vaccination of naive individuals could be a suitable strategy to limit the impact of emerging variants. This strategy is currently being evaluated for immunocompromised patients in several countries.

RBD-NP vaccine elicits cross-reactive sarbecovirus polyclonal Abs in NHPs

As RBD-NP- and HexaPro S-elicited polyclonal Abs exhibited similar resilience to a range of mutations, we next investigated cross-reactivity with a panel of sarbecovirus RBDs. RBD-NP-elicited polyclonal Abs purified from pigtail macaque serum obtained 70 days post-prime strongly cross-reacted with the SARS-CoV-2-related Pangolin-GD and RaTG13 RBDs and bound more weakly to distantly related RmYN02, SARS-CoV, WIV16, and ZXC21 RBDs (Figures S2B and S2C). Measurement of Ab binding titers using the SARS-CoV and SARS-CoV-2 S2P ectodomain trimers by ELISA showed that RBD-NPs and HexaPro S induced similar levels of cross-reactive Abs against each antigen, with responses roughly two orders of magnitude higher against SARS-CoV-2 S2P (detection antigen matching immunogen) compared to SARS-CoV S2P (Figure S2D; Data S1). The two immunogens also elicited similar peak levels of SARS-CoV S ACE2-competing Abs (GMT 2 × 10^2 RBD-NP and 5 × 10^1 HexaPro) suggesting that cross-neutralizing Abs might have been induced to similar extents between the two vaccines (Figure S2E).

Motivated by the cross-reactivity of RBD-NP-elicited polyclonal Abs with various sarbecovirus RBDs and the correlation between ACE2 competition and serum neutralization titers (Piccoli et al., 2020), we evaluated neutralization of a panel of HIV (D614G GMT 5.5 × 10^2) and VSV (D614G GMT 6 × 10^2) pseudoviruses harboring sarbecovirus S glycoproteins. RBD-NP-elicited sera efficiently neutralized pseudotyped viruses harboring the S glycoprotein of the Pangolin-GD isolate (GMT 6.6 × 10^2 and 7.7 × 10^2 VSV) and RaTG13 (GMT VSV 6 × 10^2) (Figures 3E and 3F) (Lam et al., 2020; Zhou et al., 2020b), in agreement with the close phylogenetic relationship of their RBDs with that of SARS-CoV-2 S (Figure S2B). HexaPro S-elicited NHP sera also efficiently neutralized Pangolin-GD S (GMT HIV 4.7 × 10^3 and VSV 9 × 10^2) and RaTG13 S pseudotypes (GMT VSV 4.7 × 10^3) (Figures 3E and 3F). Furthermore, we observed that both RBD-NP- and HexaPro S-induced polyclonal Abs that weakly neutralized HIV pseudovirus carrying SARS-CoV S (RBD-NP GMT 6 × 10^1 and HexaPro GMT 1 × 10^2) (Figures 3E and 3F). Collectively, these data demonstrate that both immunogens elicited comparable neutralization breadth and potency against the pseudoviruses tested, reinforcing the notion that most sarbecovirus S-directed neutralizing Abs target the RBD (Greaney et al., 2021a, 2021b; Piccoli et al., 2020).

Design, assembly, and characterization of mosaic and cocktail sarbecovirus RBD-NPs

We and others have recently evaluated nanoparticle immunogens that display multiple antigenic variants of viral glycoproteins as a potential route toward broadly protective vaccines (Boyoglu-Barnum et al., 2021; Cohen et al., 2021a, 2021b; Kanekiyo et al., 2019). Given the large number of coronaviruses circulating in zoonotic reservoirs, such vaccines could be important for understanding vaccine-induced neutralization/protection breadth and preventing future pandemics (Menachery et al., 2015, 2016). We expressed and purified four RBDs from the S proteins of SARS-CoV-2, SARS-CoV, and the bat coronaviruses WIV1 and RaTG13 genetically fused to the I53-50A trimer. An equimolar mixture of these four proteins was added to the I53-50B pentamer to assemble a mosaic RBD-NP (mRBD-NP) co-displaying the four RBDs on the same nanoparticle (Figure 4A and S3A). We also assembled a trivalent mosaic RBD-NP designated "drop out" lacking the SARS-CoV RBD (mRBD-NP-DO), as well as cocktail immunogens with three (cRBD-NP-DO; lacking the SARS-CoV RBD) or four (cRBD-NP) independently assembled nanoparticles, each displaying a single type of the aforementioned RBDs, mixed after independent assembly. Finally, we made a bivalent mosaic RBD-NP co-displaying the SARS-CoV and SARS-CoV-2 RBDs (Figure S3A) to directly confirm co-display on the nanoparticles using a sandwich binding assay. All of the nanoparticle immunogens formed the intended icosahedral architecture and retained native antigenicity, as shown by SDS-PAGE, dynamic light scattering, negative staining electron microscopy, and binding to hACE2-Fc (Figures S3B–S3E). We found that the vaccine candidates were stable for at least 4 weeks at several temperatures except the highest temperature evaluated (37°C), at which we observed a decrease in hACE2 recognition over time beginning after 7 to 14 days, presumably due to aggregation (Figures 4B–4E). Following immobilization using the SARS-CoV-2-specific mAb S2H14 (Piccoli et al., 2020), the quadrivalent, trivalent, and bivalent mRBD-NPs all bound the Fab of the SARS-CoV-specific Ab S230 (Piccoli et al., 2020; Rockx et al., 2008; Walls et al., 2019), confirming co-display, whereas the monovalent SARS-CoV-2 RBD-NP did not (Figure S3G). We determined that the reactivity of the trivalent mRBD-NP derived from the inclusion of the WIV1 RBD in this vaccine, as the monovalent WIV1 RBD-NP also bound the S230 Fab after immobilization with hACE2 (as expected [Menachery et al., 2016]), whereas the monovalent SARS-CoV-2 and RaTG13 RBD-NPs did not (Figure S3H). Collectively, these data demonstrate that all of the nanoparticles were stable and (co-)displayed the various RBDs as intended.

Cocktail and mosaic RBD-NP vaccines elicit cross-reactive and broadly neutralizing sarbecovirus Abs

The mosaic and cocktail nanoparticle immunogens were compared to monovalent RBD-NP vaccines and a non-assembling control vaccine comprising all four RBD-I53-50A trimeric components and a non-assembling I53-50B pentamer (Figure S3F) in an immunization study in BALB/c cByJ mice (Figures 4A and S3A). All immunizations comprised 1 μg of total RBD antigen, such that ~0.25 μg of each RBD was given in each administration of the quadrivalent vaccines

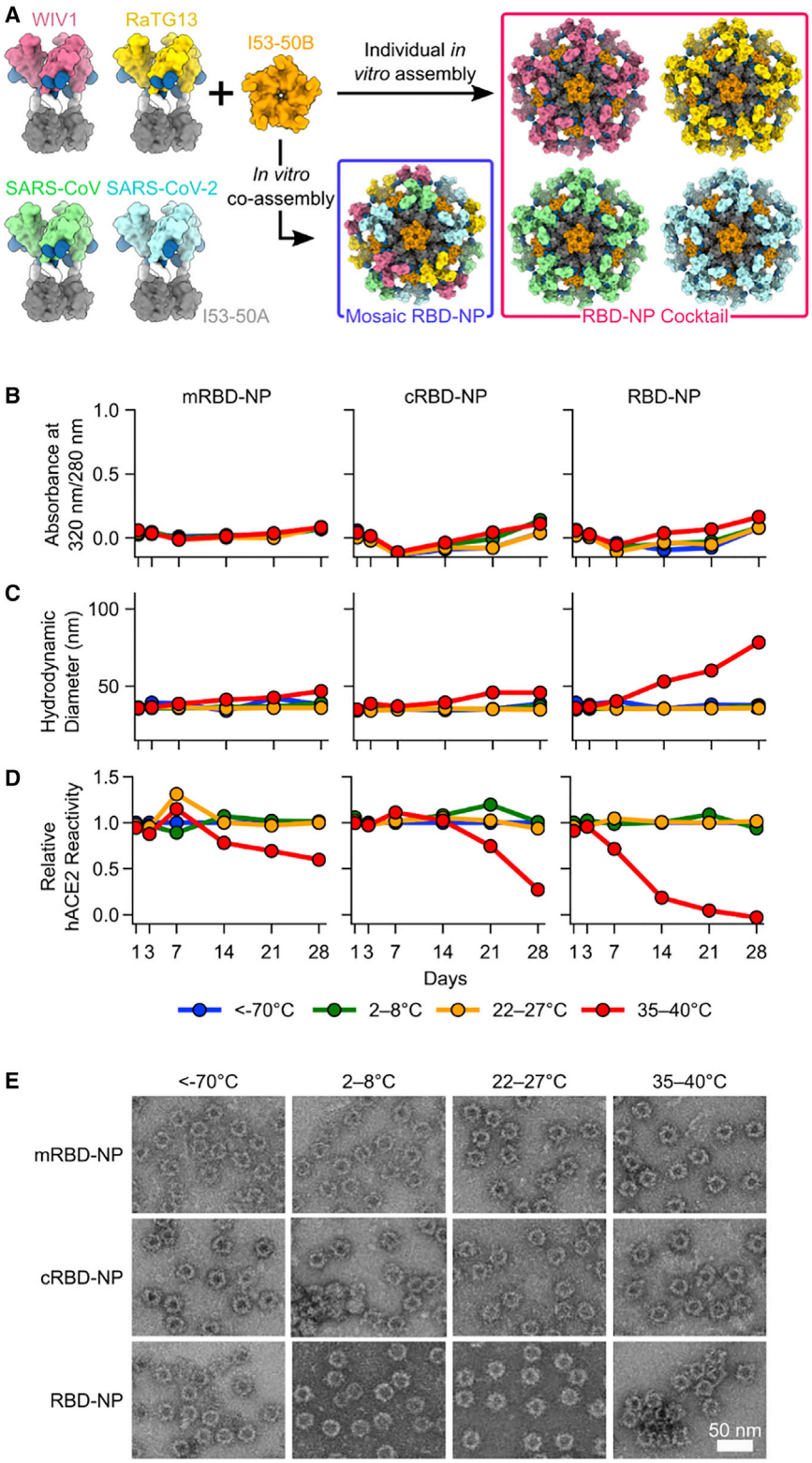

Figure 4. *In vitro* assembly and accelerated stability studies of mosaic and cocktail nanoparticle immunogens

(A) Schematic of *in vitro* assembly of mRBD-NPs and cRBD-NPs.

(B–E) The physical and antigenic stability of mRBD-NP, cRBD-NP, and (SARS-CoV-2) RBD-NP samples incubated at four different temperatures was followed for four weeks.

(B) The ratio of UV/vis absorbance at 320 nm/280 nm is a measure of turbidity (proxy for aggregation).

(C) Hydrodynamic diameter of the nanoparticles measured using dynamic light scattering.

(D) hACE2-Fc binding measured by comparing the peak amplitude of hACE2-Fc binding for each sample to a reference sample stored at < −70°C using biolayer interferometry.

(E) Electron micrographs of negatively stained samples after incubation for 28 days at the indicated temperatures. Scale bar, 50 nm.

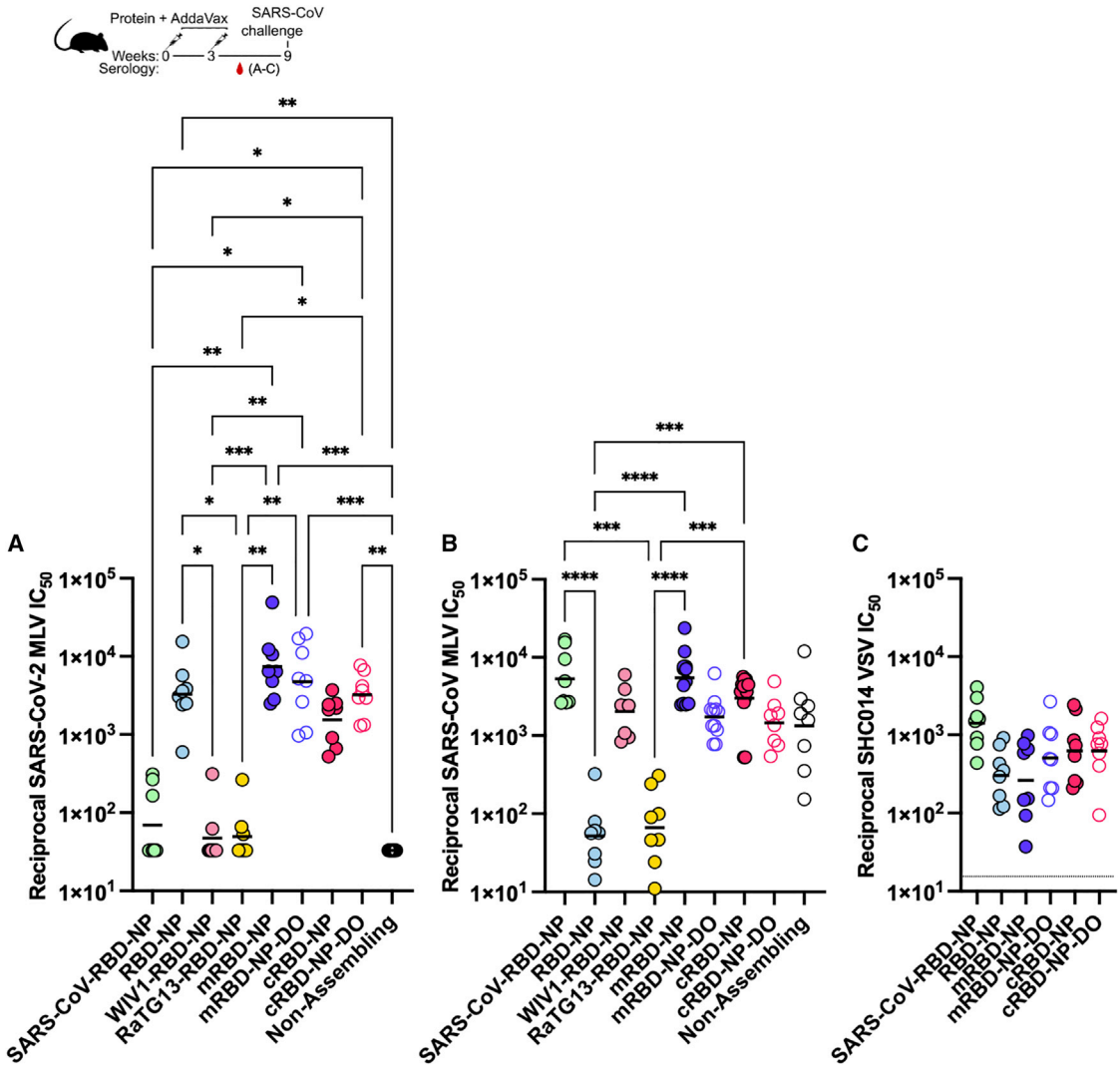

Figure 5. Mosaic and cocktail RBD-NP vaccines elicit neutralizing Abs against multiple sarbecoviruses

(A) Neutralizing Ab titers in mice (n = 8) against wild-type (D614G) SARS-CoV-2 S MLV pseudovirus five weeks post-prime elicited by monovalent, mosaic, and cocktail RBD-NPs with an LOD of 1×10^1.

(B) Neutralizing Ab titers in mice against SARS-CoV S MLV pseudovirus five weeks post-prime elicited by monovalent, mosaic, and cocktail RBD-NPs with an LOD of 1×10^1.

(C) Neutralizing Ab titers in mice against SHC014 VSV pseudovirus five weeks post-prime elicited by monovalent, mosaic, and cocktail RBD-NPs with an LOD of 1.7×10^1.

Raw data curves shown in Data S1. Statistical significance was determined by Kruskal-Wallis test and shown only when significant. **p<0.01. LOD is shown as a gray horizontal dotted line in (C).

and ~0.33 μg of each RBD in the trivalent vaccines. After two immunizations, all four mosaic or cocktail RBD-NP vaccines elicited strong binding (GMT ~1–5 × 10^4) (Figure S4A; Data S1) and potent serum neutralizing (GMT 2–8 × 10^3; Figure 5A; Data S1) Ab titers against wild-type (D614G) SARS-CoV-2 S pseudovirus. Competition ELISAs using hACE2, CR3022, S309, and S2X259 demonstrated that all mosaic and cocktail vaccine candidates elicited robust Ab titers targeting all antigenic sites tested, showcasing the diversity of RBD-specific Abs elicited (Figures S4B–S4E; Data S1). The neutralizing SARS-CoV-2 S (D614G) Ab responses were slightly higher for mRBD-NPs and slightly lower for cRBD-NPs than that of the monovalent RBD-NP (GMT 3 × 10^3) (Figure 5A), similar to the aforementioned low-dose RBD-NP immunization study (Figure 1D) and suggesting that the dose of strain-matched antigen in the multivalent vaccines is not a limiting factor of the magnitude of neutralizing Ab responses. The neutralizing activity against SARS-CoV-2 elicited by the other monovalent RBD-NPs and the non-assembling control were ~2 orders of magnitude lower (GMT < 5 × 10^1) than for the monovalent RBD-NP, indicating poor elicitation of cross-neutralizing Abs by these heterologous monovalent RBD-NPs.

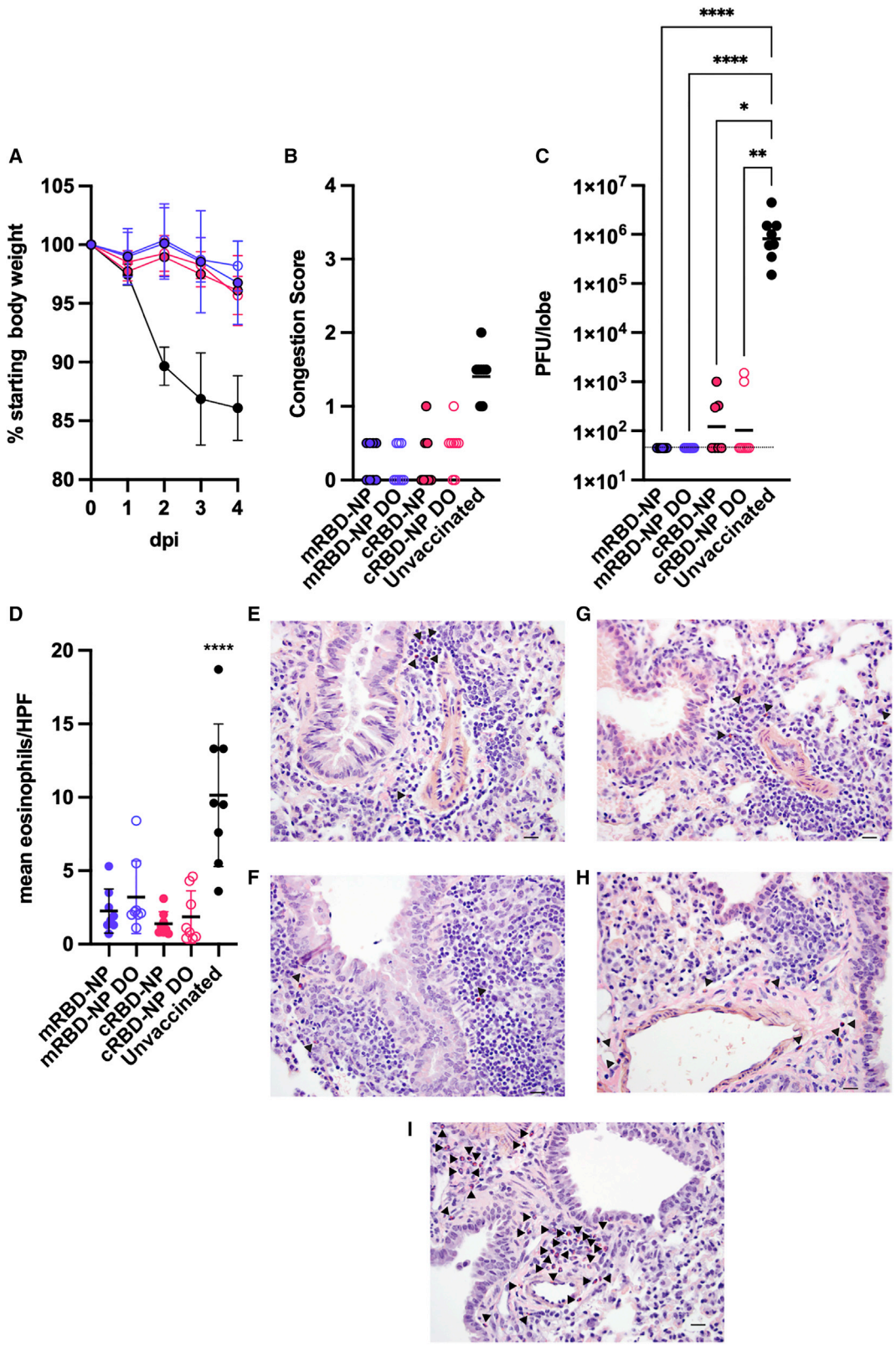

(legend on next page)

Although ELISA binding titers were comparable across mosaic and cocktail groups against SARS-CoV S2P (GMT 3–10 × 10^3), the corresponding pseudovirus neutralization titers showed more nuanced patterns (Figures 5B and S4F; Data S1). Tetravalent mosaic and cocktail RBD-NPs elicited potent neutralizing activity (GMT 3–5.5 × 10^3) with magnitudes roughly comparable to that of the monovalent SARS-CoV-RBD-NP (GMT 5 × 10^3) (Figure 5B). Strikingly, the trivalent nanoparticle immunogens (mRBD-NP-DO and cRBD-NP-DO)—which did not contain the SARS-CoV RBD—also elicited potent neutralization (GMT ~1–2 × 10^3). This cross-neutralization likely arose from the inclusion of the WIV1 RBD (Figure S4G; Data S1) in the trivalent immunogens, as WIV1 cross-reacts with a SARS-CoV-specific mAb (Figure S3H) (Menachery et al., 2016), and the monovalent WIV1-RBD-NP induced similar levels of pseudovirus neutralization (GMT 2 × 10^3) (Figure 5B; Data S1). The non-assembling control immunogen, which contains all four RBD-I53-50A trimeric components, also elicited substantial neutralizing activity against SARS-CoV (GMT 1 × 10^3) but not against SARS-CoV-2. Furthermore, we show that sera elicited by the monovalent, mRBD-NPs, and cRBD-NPs neutralize SHC014 pseudotyped virus, a distantly related sarbecovirus sharing 76%, 76%, 82%, and 84% amino acid sequence identity with the SARS-CoV-2, RaTG13, SARS-CoV, and WIV1 RBDs, respectively (Figure 5C; Data S1). These data show that both mRBD-NPs and cRBD-NPs are promising vaccine candidates for eliciting broad sarbecovirus immunity, in agreement with previous findings using a different nanoparticle platform (Cohen et al., 2021a) or chimeric sarbecovirus S glycoproteins (Martinez et al., 2021b) and recent results obtained with influenza virus hemagglutinin nanoparticle vaccines (Boyoglu-Barnum et al., 2021).

Mosaic RBD-NPs protect mice against heterotypic SARS-CoV challenge

To gauge the ability of the multivalent RBD-NPs to confer protection against vaccine-matched and heterotypic sarbecoviruses, we challenged groups of eight mice with a high dose (10^5 PFUs) of the mouse-adapted SARS-CoV MA15 virus (Roberts et al., 2007). In agreement with the pseudovirus neutralization data, animals immunized with mRBD-NP, mRBD-NP-DO, cRBD-NP, and cRBD-NP-DO were protected from weight loss (ranging between 1% and 5%) and serious lung pathology throughout the four days of the experiment (Figures 6A and 6B). Unvaccinated mice exhibited up to 15% average weight loss and signs of lung pathology (congestion score ~1.5) that were only minorly seen in all other vaccinated groups (Figures 6A and 6B). mRBD-NP- and mRBD-NP-DO-vaccinated mice were completely protected from viral replication in the lungs (Figure 6C). Overall, the trivalent mRBD-NP-DO provided protection that was indistinguishable from the tetravalent mRBD-NP, despite lacking the SARS-CoV RBD. Five out of eight and six out of eight cRBD-NP- and cRBD-NP-DO-vaccinated mice were completely protected from viral replication in the lungs, respectively, with viral burden ranging between 10^2 and 10^3 PFUs/lobe for the remaining animals (compared to unvaccinated mice with ~10^6 PFUs/lobe, Figure 6C). To assess whether the RBD-NP platform causes vaccine-induced immune pathology, which was previously described with double-inactivated SARS-CoV vaccines (Bolles et al., 2011), we investigated eosinophil infiltration and inflammation in the lungs following SARS-CoV MA15 challenge. Although infection induced inflammation and infiltration of eosinophils in the lungs of unvaccinated mice (Figures 6D, 6I, and S5A), no signs of eosinophilia were detected for any animals in the vaccinated groups using histological analysis of stained lung sections (Figures 6D–6I and S5A). These data show that mRBD-NP, mRBD-NP-DO, cRBD-NP, and cRBD-NP-DO protect against weight loss, lung injury, and viral replication following challenge, with no detectable vaccine-induced immune pathology.

To identify the gain in protective breadth provided by multivalent display of sarbecovirus RBD-NP, relative to monovalent RBD-NPs, we performed a second SARS-CoV MA15 challenge experiment including monovalent RBD-NP and SARS-CoV-RBD-NP (Figure S5B). In agreement with the pseudovirus neutralization data and first challenge (Figures 4B–4D and 6A–6C), animals immunized with the SARS-CoV-RBD-NP, mosaic, and cocktail RBD-NP formulations, as well as the non-assembling control immunogen, were protected from weight loss and serious lung pathology throughout the four days of the experiment. The animals receiving the monovalent RBD-NP vaccine experienced up to 12% average weight loss, whereas the unvaccinated mice exhibited further (up to 15%) average weight loss and signs of lung pathology (congestion score ~2) that were only minorly seen in all other vaccinated groups (Figures S5B and S5C). All mice vaccinated with SARS-CoV-RBD-NP, RBD-NP, and mRBD-NP were protected from viral replication in the lungs, whereas we detected ~$10^{2.5}$ and 10^6 PFUs/lobe for half of the mice receiving the non-assembling control immunogen and unvaccinated mice, respectively (Figure S5D). These results provide proof-of-principle that mosaic and cocktail RBD nanoparticle vaccines elicit broad protection against heterotypic sarbecovirus challenge and could represent the next generation of vaccines developed in anticipation of future spillovers.

Figure 6. Mosaic and cocktail RBD-NP vaccines protect against heterotypic SARS-CoV-MA15 challenge in 15-week-old BALB/c cByJ mice

(A) Weight loss following SARS-CoV MA15 challenge up to 4 days post infection (n = 8). Unvaccinated animals are shown as black circles.

(B) Congestion score following SARS-CoV MA15 infection with a score of 0 indicating unchanged lung color and 4 indicating a darkened and diseased lung (n = 8).

(C) Viral titers in mice lungs (expressed in PFUs per lobe) following challenge (n = 8) with an LOD of 9 × 10^1. LOD is shown as a gray horizontal dotted line. Statistical significance was determined by Kruskal-Wallis and shown when significant. **$p < 0.01$.

(D) Mean eosinophils per high power field (HPF) per sample run over 10 HPF per lung stained with congo red. Significance was determined using one-way ANOVA and shown where significant.

(E–I) Histological analysis of stained lung sections for mRBD-NP (E), mRBD-NP-DO (F), cRBD-NP (G), cRBD-NP-DO (H), and unvaccinated mice (I). Arrowheads indicate eosinophils. Scale bar, 20 μm.

DISCUSSION

The data presented here show that two ultra-low dose immunizations or a single immunization with RBD-NP produces potent neutralizing Ab responses in mice. The latter strategy confers protection against SARS-CoV-2 MA10 challenge, suggesting that the nanoparticle platform could enable dose-sparing regimens to achieve global vaccination, especially given the high shelf stability of this vaccine (Walls et al., 2020b). NHP vaccination with RBD-NP was concurrently shown to also elicit CD4 T cell responses and to protect from viral replication (Arunachalam et al., 2021). Moreover, RBD-NP vaccination, which is currently under phase I/II evaluation in the clinic, elicits diverse Ab responses neutralizing a broad spectrum of SARS-CoV-2 variants detected in clinical isolates with similar potency to those elicited by HexaPro S vaccination. Several RBM mutations, including at position E484, however, lead to reductions in neutralizing activity elicited by either RBD-NP or HexaPro S in NHPs. Although both RBD-NP- and HexaPro S-elicited sera robustly neutralize the B.1.1.7 S variant, which does not contain the E484 substitution, neutralization of the B.1.351, P.1, and B.1.1.7/E484K variants was dampened similarly to sera from individuals vaccinated twice with the Pfizer-BioNTech BNT162b2 mRNA. These findings are in agreement with reports showing that the serum neutralizing activity against the B.1.351 variant from mRNA-1273-vaccinated individuals was comparably reduced (Wu et al., 2021), as was also the case for neutralization of authentic SARS-CoV-2 B.1.351 by HCP (Wibmer et al., 2021). Collectively, these data indicate that a significant fraction of vaccine-elicited neutralizing activity is directed to the RBM, which is the target of potent neutralizing Abs, irrespective of the antigen design strategy (RBD- or S-based), the vaccine modality (protein subunit or mRNA), or species (NHPs or humans). We show that receiving a third immunization, even of an unaltered vaccine, improves the neutralizing Ab responses to VOCs, which is reminiscent of what has been shown in vaccinated humans previously infected with SARS-CoV-2 (Abu Jabal et al., 2021; Krammer et al., 2021; Stamatatos et al., 2021), suggesting that further booster immunizations may limit the impact of VOCs without vaccine update.

The ongoing global spread of SARS-CoV-2 and the circulation of a large number of sarbecoviruses in bats (Menachery et al., 2015, 2016) and other animal reservoirs strongly motivate the development of vaccines that protect against a broad spectrum of coronaviruses. We observed that vaccination of NHPs with RBD-NPs or HexaPro S induced comparable but moderate neutralization breadth against genetically distinct sarbecoviruses. We demonstrate here that co-display (mRBD-NP) and co-immunization (cRBD-NP) of multivalently arrayed sarbecovirus RBDs elicit robust neutralizing Ab responses against SARS-CoV-2, SARS-CoV, and SHC014 pseudotyped viruses and outperform their monovalent vaccine counterparts. The observation that mosaic and cocktail RBD-NPs elicit greater titers of Abs competing with the broadly neutralizing sarbecovirus mAb S2X259 than monovalent vaccines suggest that this vaccine design strategy could enhance neutralization breadth. Accordingly, mice vaccinated with multivalent vaccines were protected from disease upon SARS-CoV MA15 challenge, including with formulations that did not include the SARS-CoV RBD, whereas RBD-NP-vaccinated mice experienced weight loss. Previous studies showed that double-inactivated SARS-CoV vaccines could lead to eosinophil infiltration in the lungs and subsequent immune pathology (Bolles et al., 2011). Our data show that none of the multivalent vaccine candidates evaluated here induced eosinophilia whereas SARS-CoV MA15 challenge did, pointing to the safety and efficacy of these immunogens. Our data highlight the potential of this approach to achieve broad sarbecovirus immunity, overcoming both the emergence of SARS-CoV-2 variants and putative future zoonosis of genetically distinct sarbecoviruses not included in the vaccine. Based on the RBD-centric nature of neutralizing Ab responses resulting from infection and vaccination (Dejnirattisai et al., 2021; Greaney et al., 2021a, 2021b; Piccoli et al., 2020), irrespective of immunogen format or vaccine modality, and the enhanced elicitation of Abs targeting all RBD antigenic sites for multivalent RBD-NPs compared to S-based vaccines, this study paves the way for advancing RBD pan-sarbecovirus subunit vaccines to the clinic.

Limitations of study

Due to the cost of challenge and BSL-3 vivarium limitations, the mice vaccinated with a low dose of RBD-NP were not challenged, and therefore we can only infer the likelihood of protection from their sera's ability to neutralize SARS-CoV-2 pseudovirus better than other mice (i.e., those given a single vaccine dose) that were challenged. Neutralization is a correlate of protection in NHPs (Arunachalam et al., 2021), but we recognize that neutralization assays using HEK-ACE2 cell lines may underestimate the effects of non-RBM targeting Abs (Lempp et al., 2021; McCallum et al., 2021a; Suryadevara et al., 2021). Due to the limitations of the number of animals and the cost of challenge, we cannot challenge with all desired point mutant or variant strains and must use neutralization as the best correlate for interpreting the expected challenge outcome.

STAR★METHODS

Detailed methods are provided in the online version of this paper and include the following:

- KEY RESOURCES TABLE
- RESOURCE AVAILABILITY
  - Lead contact
  - Materials availability
  - Data and code availability
- EXPERIMENTAL MODEL AND SUBJECT DETAILS
  - Cell lines
  - Mice
  - Pigtail macaques
  - Rhesus macaques
  - Convalescent human sera
  - Pfizer vaccinated human sera
- METHOD DETAILS
  - Plasmid construction
  - Transient transfection
  - Microbial protein expression and purification

- Protein purification
- *In vitro* nanoparticle assembly and purification
- Endotoxin measurements
- Pigtail macaque immunization
- Rhesus macaque immunization
- Deep mutational scanning
- ELISA
- Competition ELISA of NHP sera with hACE2, CR3022 IgG, and S309 IgG for immobilized SARS-CoV-2 S2P
- Competition ELISA of mouse sera and immobilized hACE2 or mAbs with SARS-CoV-2 or SARS-CoV S2P
- Pseudovirus production
- Pseudovirus neutralization
- Sarbecovirus biolayer interferometry binding analysis
- Cocktail and mosaic bio-layer interferometry (antigenicity)
- Sandwich bio-layer interferometry (mosaic display antigenicity)
- Cocktail and mosaic negative stain electron microscopy
- Cocktail and mosaic dynamic light scattering
- Mouse immunizations and challenge
- Histopathology of post challenge mouse lungs

● QUANTIFICATION AND STATISTICAL ANALYSIS

SUPPLEMENTAL INFORMATION

Supplemental information can be found online at https://doi.org/10.1016/j.cell.2021.09.015.

ACKNOWLEDGMENTS

We thank Helen Chu and Marion Pepper for coordination of HCP samples and Ratika Krishnamurty for program management. The authors thank Kathryn Guerriero, Brieann Brown, Solomon Wangari, Joel Ahrens, Naoto Iwayama, and William Garrison for their technical assistance with the pigtail macaque study. This study was supported by the Bill and Melinda Gates Foundation (INV–017592 to J.S.M. and OPP1156262 to N.P.K. and D.V.); generous gifts from the Audacious Project, Jodi Green and Mike Halperin, and the Hanauer family; the Defense Threat Reduction Agency (HDTRA1-18-1-0001 to N.P.K.); the National Institute of General Medical Sciences(R01GM120553 to D.V.); National Institute of Health Office of Research Infrastructure Programs (P51-OD010425, Washington National Primate Research Center); the National Institute of Allergy and Infectious Diseases (R01-AI127521 to J.S.M. and DP1AI158186 and HHSN272201700059C to D.V.); the National Institute of General Medical Sciences (R01GM120553 to D.V. and 5T32GM008268-32 to S.K.Z.); a Pew Biomedical Scholars Award (D.V.); Investigators in the Pathogenesis of Infectious Disease Awards from the Burroughs Wellcome Fund (D.V.); Fast Grants (D.V.); Animal Models contracts HHSN272201700036I-75N93020F00001 and U01 AI149644 (R.S.B.); and the North Carolina Policy Collaboratory at the University of North Carolina at Chapel Hill with funding from the North Carolina Coronavirus Relief Fund, established and appropriated by the North Carolina General Assembly (R.S.B.). D.R.M. is currently supported by a Burroughs Wellcome Fund Postdoctoral Enrichment Program Award and a Hanna H. Gray Fellowship from the Howard Hughes Medical Institute and was supported by an NIH NIAID T32 AI007151 and an NIAID F32 AI152296.

AUTHOR CONTRIBUTIONS

Conceptualization, A.C.W., P.S.A., H.K., B.P., N.P.K., D.V.; modeling and design, A.C.W., N.P.K., D.V.; formal analysis, A.C.W., M.C.M., A.S., A.G., M.A.T., J.B., B.F., M.J.N., S.W., T.S., R.R., C.S., L.C., N.P.K, D.V.; resources, M.A.O., P.S.A., S.W.T., R.R., D.T.O., R.V.D.M., R.S.B., W.V.W., D.C., C.-L.H., J.S.M., D.H.F., F.V., B.P.; writing – original draft, A.C.W., N.P.K., D.V.; writing – review & editing, all authors; visualization, A.C.W., M.C.M., A.S., A.G., N.B., N.P.K., R.S.B., D.V.; supervision, D.H.F., J.S.M., L.C., R.S.B., T.P.S., B.P., N.P.K., D.V.; funding acquisition, J.S.M., R.S.B., N.P.K., D.V.

DECLARATION OF INTERESTS

A.C.W., N.P.K., and D.V. are named as inventors on patent applications filed by the University of Washington based on the studies presented in this paper. N.P.K. is a co-founder, shareholder, paid consultant, and chair of the scientific advisory board of Icosavax, Inc. and has received an unrelated sponsored research agreement from Pfizer. D.C. is an employee of Vir Biotechnology and may hold shares in Vir Biotechnology. D.V. is a consultant for and has received an unrelated sponsored research agreement from Vir Biotechnology, Inc. R.R., D.T.O., and R.V.D.M. are employees of GlaxoSmithKline. C.-L.H. and J.S.M. are inventors on US patent application no. 63/032,502, "Engineered Coronavirus Spike (S) Protein and Methods of Use Thereof". R.S.B. has collaborative research agreements with Takeda, Pfizer, Eli Lily, Gilead, Ridgeback Biosciences, and VaxArt, unrelated to the current research. The other authors declare no competing interests.

Received: April 5, 2021
Revised: June 18, 2021
Accepted: September 9, 2021
Published: September 15, 2021

REFERENCES

Abu Jabal, K., Ben-Amram, H., Beiruti, K., Batheesh, Y., Sussan, C., Zarka, S., and Edelstein, M. (2021). Impact of age, ethnicity, sex and prior infection status on immunogenicity following a single dose of the BNT162b2 mRNA COVID-19 vaccine: real-world evidence from healthcare workers, Israel, December 2020 to January 2021. Euro Surveill. *26*, 2100096.

Andreano, E., Piccini, G., Licastro, D., Casalino, L., Johnson, N.V., Paciello, I., Monego, S.D., Pantano, E., Manganaro, N., Manenti, A., et al. (2020). SARS-CoV-2 escape in vitro from a highly neutralizing COVID-19 convalescent plasma. bioRxiv, 2020.12.28.424451.

Arunachalam, P.S., Walls, A.C., Golden, N., Atyeo, C., Fischinger, S., Li, C., Aye, P., Navarro, M.J., Lai, L., Edara, V.V., et al. (2021). Adjuvanting a subunit COVID-19 vaccine to induce protective immunity. Nature *594*, 253–258.

Avanzato, V.A., Matson, M.J., Seifert, S.N., Pryce, R., Williamson, B.N., Anzick, S.L., Barbian, K., Judson, S.D., Fischer, E.R., Martens, C., et al. (2020). Case Study: Prolonged infectious SARS-CoV-2 shedding from an asymptomatic immunocompromised cancer patient. Cell *183*, 1901, 1012.e9.

Bale, J.B., Gonen, S., Liu, Y., Sheffler, W., Ellis, D., Thomas, C., Cascio, D., Yeates, T.O., Gonen, T., King, N.P., and Baker, D. (2016). Accurate design of megadalton-scale two-component icosahedral protein complexes. Science *353*, 389–394.

Barnes, C.O., Jette, C.A., Abernathy, M.E., Dam, K.A., Esswein, S.R., Gristick, H.B., Malyutin, A.G., Sharaf, N.G., Huey-Tubman, K.E., Lee, Y.E., et al. (2020). SARS-CoV-2 neutralizing antibody structures inform therapeutic strategies. Nature *588*, 682–687.

Baum, A., Ajithdoss, D., Copin, R., Zhou, A., Lanza, K., Negron, N., Ni, M., Wei, Y., Mohammadi, K., Musser, B., et al. (2020a). REGN-COV2 antibodies prevent and treat SARS-CoV-2 infection in rhesus macaques and hamsters. Science *370*, 1110–1115.

Baum, A., Fulton, B.O., Wloga, E., Copin, R., Pascal, K.E., Russo, V., Giordano, S., Lanza, K., Negron, N., Ni, M., et al. (2020b). Antibody cocktail to SARS-CoV-2 spike protein prevents rapid mutational escape seen with individual antibodies. Science *369*, 1014–1018.

Bolles, M., Deming, D., Long, K., Agnihothram, S., Whitmore, A., Ferris, M., Funkhouser, W., Gralinski, L., Totura, A., Heise, M., and Baric, R.S. (2011). A double-inactivated severe acute respiratory syndrome coronavirus vaccine provides incomplete protection in mice and induces increased eosinophilic

proinflammatory pulmonary response upon challenge. J. Virol. *85*, 12201–12215.

Boyoglu-Barnum, S., Ellis, D., Gillespie, R.A., Hutchinson, G.B., Park, Y.-J., Moin, S.M., Acton, O.J., Ravichandran, R., Murphy, M., Pettie, D., et al. (2021). Quadrivalent influenza nanoparticle vaccines induce broad protection. Nature *592*, 623–628.

Brouwer, P.J.M., Caniels, T.G., van der Straten, K., Snitselaar, J.L., Aldon, Y., Bangaru, S., Torres, J.L., Okba, N.M.A., Claireaux, M., Kerster, G., et al. (2020). Potent neutralizing antibodies from COVID-19 patients define multiple targets of vulnerability. Science *369*, 643–650.

Cathcart, A.L., Havenar-Daughton, C., Lempp, F.A., Ma, D., Schmid, M., Agostini, M.L., Guarino, B., Di iulio, J., Rosen, L., Tucker, H., et al. (2021). The dual function monoclonal antibodies VIR-7831 and VIR-7832 demonstrate potent in vitro and in vivo activity against SARS-CoV-2. bioRxiv. https://doi.org/10.1101/2021.03.09.434607.

Choi, B., Choudhary, M.C., Regan, J., Sparks, J.A., Padera, R.F., Qiu, X., Solomon, I.H., Kuo, H.H., Boucau, J., Bowman, K., et al. (2020). Persistence and Evolution of SARS-CoV-2 in an Immunocompromised Host. N. Engl. J. Med. *383*, 2291–2293.

Cohen, A.A., Gnanapragasam, P.N.P., Lee, Y.E., Hoffman, P.R., Ou, S., Kakutani, L.M., Keeffe, J.R., Wu, H.-J., Howarth, M., West, A.P., et al. (2021a). Mosaic nanoparticles elicit cross-reactive immune responses to zoonotic coronaviruses in mice. Science *371*, 735–741.

Cohen, A.A., Yang, Z., Gnanapragasam, P.N.P., Ou, S., Dam, K.A., Wang, H., and Bjorkman, P.J. (2021b). Construction, characterization, and immunization of nanoparticles that display a diverse array of influenza HA trimers. PLoS ONE *16*, e0247963.

Collier, D.A., De Marco, A., Ferreira, I.A.T.M., Meng, B., Datir, R.P., Walls, A.C., Kemp, S.A., Bassi, J., Pinto, D., Silacci-Fregni, C., et al.; CITIID-NIHR BioResource COVID-19 Collaboration; COVID-19 Genomics UK (COG-UK) Consortium (2021). Sensitivity of SARS-CoV-2 B.1.1.7 to mRNA vaccine-elicited antibodies. Nature *593*, 136–141.

Corbett, K.S., Edwards, D.K., Leist, S.R., Abiona, O.M., Boyoglu-Barnum, S., Gillespie, R.A., Himansu, S., Schäfer, A., Ziwawo, C.T., DiPiazza, A.T., et al. (2020a). SARS-CoV-2 mRNA vaccine design enabled by prototype pathogen preparedness. Nature *586*, 567–571.

Corbett, K.S., Flynn, B., Foulds, K.E., Francica, J.R., Boyoglu-Barnum, S., Werner, A.P., Flach, B., O'Connell, S., Bock, K.W., Minai, M., et al. (2020b). Evaluation of the mRNA-1273 Vaccine against SARS-CoV-2 in Nonhuman Primates. N. Engl. J. Med. *383*, 1544–1555.

Crawford, K.H.D., Eguia, R., Dingens, A.S., Loes, A.N., Malone, K.D., Wolf, C.R., Chu, H.Y., Tortorici, M.A., Veesler, D., Murphy, M., et al. (2020). Protocol and Reagents for Pseudotyping Lentiviral Particles with SARS-CoV-2 Spike Protein for Neutralization Assays. Viruses *12*, 513.

Davies, N.G., Barnard, R.C., Jarvis, C.I., Kucharski, A.J., Munday, J., Pearson, C.A.B., Russell, T.W., Tully, D.C., Abbott, S., Gimma, A., et al. (2020). Estimated transmissibility and severity of novel SARS-CoV-2 Variant of Concern 202012/01 in England. medRxiv. https://doi.org/10.1101/2020.12.24.20248822.

Dejnirattisai, W., Zhou, D., Ginn, H.M., Duyvesteyn, H.M.E., Supasa, P., Case, J.B., Zhao, Y., Walter, T.S., Mentzer, A.J., Liu, C., et al. (2021). The antigenic anatomy of SARS-CoV-2 receptor binding domain. Cell *184*, 2183–2200.e22.

Deng, X., Garcia-Knight, M.A., Khalid, M.M., Servellita, V., Wang, C., Morris, M.K., Sotomayor-González, A., Glasner, D.R., Reyes, K.R., Gliwa, A.S., et al. (2021). Transmission, infectivity, and neutralization of a spike L452R SARS-CoV-2 variant. Cell *184*, 3426–3437.e8.

Dinnon, K.H., 3rd, Leist, S.R., Schäfer, A., Edwards, C.E., Martinez, D.R., Montgomery, S.A., West, A., Yount, B.L., Jr., Hou, Y.J., Adams, L.E., et al. (2020). A mouse-adapted model of SARS-CoV-2 to test COVID-19 countermeasures. Nature *586*, 560–566.

Dong, J., Zost, S.J., Greaney, A.J., Starr, T.N., Dingens, A.S., Chen, E.C., Chen, R.E., Case, J.B., Sutton, R.E., Gilchuk, P., et al. (2021). Genetic and structural basis for recognition of SARS-CoV-2 spike protein by a two-antibody cocktail. bioRxiv. https://doi.org/10.1101/2021.01.27.428529.

Faria, N.R., Claro, I.M., Candido, D., Moyses Franco, L.A., Andrade, P.S., Coletti, T.M., Silva, C.A.M., Sales, F.C., Manuli, E.R., Aguiar, R.S., et al. (2021). Genomic characterisation of an emergent SARS-CoV-2 lineage in Manaus: preliminary findings. https://virological.org/t/genomic-characterisation-of-an-emergent-sars-cov-2-lineage-in-manaus-preliminary-findings/586.

Gibson, D.G., Young, L., Chuang, R.Y., Venter, J.C., Hutchison, C.A., 3rd, and Smith, H.O. (2009). Enzymatic assembly of DNA molecules up to several hundred kilobases. Nat. Methods *6*, 343–345.

Greaney, A.J., Starr, T.N., Gilchuk, P., Zost, S.J., Binshtein, E., Loes, A.N., Hilton, S.K., Huddleston, J., Eguia, R., Crawford, K.H.D., et al. (2020). Complete Mapping of Mutations to the SARS-CoV-2 Spike Receptor-Binding Domain that Escape Antibody Recognition. Cell Host Microbe *29*, 44–57.e9.

Greaney, A.J., Loes, A.N., Gentles, L.E., Crawford, K.H.D., Starr, T.N., Malone, K.D., Chu, H.Y., and Bloom, J.D. (2021a). Antibodies elicited by mRNA-1273 vaccination bind more broadly to the receptor binding domain than do those from SARS-CoV-2 infection. Sci. Transl. Med. *13*, 13.

Goddard, T.D., Huang, C.C., Meng, E.C., Pettersen, E.F., Couch, G.S., Morris, J.H., and Ferrin, T.E. (2018). UCSF ChimeraX: Meeting modern challenges in visualization and analysis. Protein Sci. *27*, 14–25.

Greaney, A.J., Loes, A.N., Crawford, K.H.D., Starr, T.N., Malone, K.D., Chu, H.Y., and Bloom, J.D. (2021b). Comprehensive mapping of mutations in the SARS-CoV-2 receptor-binding domain that affect recognition by polyclonal human plasma antibodies. Cell Host Microbe *29*, 463–476.e6.

Hoffmann, M., Kleine-Weber, H., Schroeder, S., Krüger, N., Herrler, T., Erichsen, S., Schiergens, T.S., Herrler, G., Wu, N.H., Nitsche, A., et al. (2020). SARS-CoV-2 Cell Entry Depends on ACE2 and TMPRSS2 and Is Blocked by a Clinically Proven Protease Inhibitor. Cell *181*, 271–280.e8.

Hou, Y.J., Chiba, S., Halfmann, P., Ehre, C., Kuroda, M., Dinnon, K.H., 3rd, Leist, S.R., Schäfer, A., Nakajima, N., Takahashi, K., et al. (2020). SARS-CoV-2 D614G variant exhibits efficient replication ex vivo and transmission in vivo. Science *370*, 1464–1468.

Hsieh, C.L., Goldsmith, J.A., Schaub, J.M., DiVenere, A.M., Kuo, H.C., Javanmardi, K., Le, K.C., Wrapp, D., Lee, A.G., Liu, Y., et al. (2020). Structure-based design of prefusion-stabilized SARS-CoV-2 spikes. Science *369*, 1501–1505.

Huo, J., Zhao, Y., Ren, J., Zhou, D., Duyvesteyn, H.M.E., Ginn, H.M., Carrique, L., Malinauskas, T., Ruza, R.R., Shah, P.N.M., et al. (2020). Neutralisation of SARS-CoV-2 by destruction of the prefusion Spike. Cell Host Microbe *28*, 445–454.e6.

Jackson, L.A., Anderson, E.J., Rouphael, N.G., Roberts, P.C., Makhene, M., Coler, R.N., McCullough, M.P., Chappell, J.D., Denison, M.R., Stevens, L.J., et al. (2020). An mRNA Vaccine against SARS-CoV-2 - Preliminary Report. N. Engl. J. Med. *383*, 1920–1931.

Jette, C.A., Cohen, A.A., Gnanapragasam, P.N.P., Muecksch, F., Lee, Y.E., Huey-Tubman, K.E., Schmidt, F., Hatziioannou, T., Bieniasz, P.D., Nussenzweig, M.C., et al. (2021). Broad cross-reactivity across sarbecoviruses exhibited by a subset of COVID-19 donor-derived neutralizing antibodies. bioRxiv. https://doi.org/10.1101/2021.04.23.441195.

Kaname, Y., Tani, H., Kataoka, C., Shiokawa, M., Taguwa, S., Abe, T., Moriishi, K., Kinoshita, T., and Matsuura, Y. (2010). Acquisition of complement resistance through incorporation of CD55/decay-accelerating factor into viral particles bearing baculovirus GP64. J. Virol. *84*, 3210–3219.

Kanekiyo, M., Joyce, M.G., Gillespie, R.A., Gallagher, J.R., Andrews, S.F., Yassine, H.M., Wheatley, A.K., Fisher, B.E., Ambrozak, D.R., Creanga, A., et al. (2019). Mosaic nanoparticle display of diverse influenza virus hemagglutinins elicits broad B cell responses. Nat. Immunol. *20*, 362–372.

Korber, B., Fischer, W.M., Gnanakaran, S., Yoon, H., Theiler, J., Abfalterer, W., Hengartner, N., Giorgi, E.E., Bhattacharya, T., Foley, B., et al.; Sheffield COVID-19 Genomics Group (2020). Tracking Changes in SARS-CoV-2 Spike: Evidence that D614G Increases Infectivity of the COVID-19 Virus. Cell *182*, 812–827.e19.

Krammer, F., Srivastava, K., and the PARIS team, and Simon, V. (2021). Robust spike antibody responses and increased reactogenicity in seropositive individuals after a single dose of SARS-CoV-2 mRNA vaccine. medRxiv. https://doi.org/10.1101/2021.01.2921250653.

Lam, T.T., Jia, N., Zhang, Y.W., Shum, M.H., Jiang, J.F., Zhu, H.C., Tong, Y.G., Shi, Y.X., Ni, X.B., Liao, Y.S., et al. (2020). Identifying SARS-CoV-2-related coronaviruses in Malayan pangolins. Nature *583*, 282–285.

Lan, J., Ge, J., Yu, J., Shan, S., Zhou, H., Fan, S., Zhang, Q., Shi, X., Wang, Q., Zhang, L., and Wang, X. (2020). Structure of the SARS-CoV-2 spike receptor-binding domain bound to the ACE2 receptor. Nature *581*, 215–220.

Leist, S.R., Dinnon, K.H., 3rd, Schäfer, A., Tse, L.V., Okuda, K., Hou, Y.J., West, A., Edwards, C.E., Sanders, W., Fritch, E.J., et al. (2020). A Mouse-Adapted SARS-CoV-2 Induces Acute Lung Injury and Mortality in Standard Laboratory Mice. Cell *183*, 1070–1085.e12.

Lempp, F.A., Soriaga, L., Montiel-Ruiz, M., Benigni, F., Noack, J., Park, Y.-J., Bianchi, S., Walls, A.C., Bowen, J.E., Zhou, J., et al. (2021). Membrane lectins enhance SARS-CoV-2 infection and influence the neutralizing activity of different classes of antibodies. bioRxiv. https://doi.org/10.1101/2021.04.03.438258.

Letko, M., Marzi, A., and Munster, V. (2020). Functional assessment of cell entry and receptor usage for SARS-CoV-2 and other lineage B betacoronaviruses. Nat. Microbiol. *5*, 562–569.

Li, Q., Wu, J., Nie, J., Zhang, L., Hao, H., Liu, S., Zhao, C., Zhang, Q., Liu, H., Nie, L., et al. (2020). The Impact of Mutations in SARS-CoV-2 Spike on Viral Infectivity and Antigenicity. Cell *182*, 1284–1294.e9.

Liu, Z., VanBlargan, L.A., Bloyet, L.-M., Rothlauf, P.W., Chen, R.E., Stumpf, S., Zhao, H., Errico, J.M., Theel, E.S., Liebeskind, M.J., et al. (2021). Identification of SARS-CoV-2 spike mutations that attenuate monoclonal and serum antibody neutralization. Cell Host Microbe *29*, 477–488.e4.

Martinez, D.R., Schaefer, A., Gobeil, S., Li, D., De la Cruz, G., Parks, R., Lu, X., Barr, M., Manne, K., Mansouri, K., et al. (2021a). A broadly neutralizing antibody protects against SARS-CoV, pre-emergent bat CoVs, and SARS-CoV-2 variants in mice. bioRxiv. https://doi.org/10.1101/2021.04.27.441655.

Martinez, D.R., Schäfer, A., Leist, S.R., De la Cruz, G., West, A., Atochina-Vasserman, E.N., Lindesmith, L.C., Pardi, N., Parks, R., Barr, M., et al. (2021b). Chimeric spike mRNA vaccines protect against Sarbecovirus challenge in mice. Science *373*, 991–998.

McCallum, M., De Marco, A., Lempp, F.A., Tortorici, M.A., Pinto, D., Walls, A.C., Beltramello, M., Chen, A., Liu, Z., Zatta, F., et al. (2021a). N-terminal domain antigenic mapping reveals a site of vulnerability for SARS-CoV-2. Cell *184*, 2332–2347.e16.

McCallum, M., Bassi, J., De Marco, A., Chen, A., Walls, A.C., Di Iulio, J., Tortorici, M.A., Navarro, M.-J., Silacci-Fregni, C., Saliba, C., et al. (2021b). SARS-CoV-2 immune evasion by the B.1.427/B.1.429 variant of concern. Science *373*, 648–654.

McCarthy, K.R., Rennick, L.J., Nambulli, S., Robinson-McCarthy, L.R., Bain, W.G., Haidar, G., and Duprex, W.P. (2021). Recurrent deletions in the SARS-CoV-2 spike glycoprotein drive antibody escape. Science *371*, 1139–1142.

McMahan, K., Yu, J., Mercado, N.B., Loos, C., Tostanoski, L.H., Chandrashekar, A., Liu, J., Peter, L., Atyeo, C., Zhu, A., et al. (2021). Correlates of protection against SARS-CoV-2 in rhesus macaques. Nature *590*, 630–634.

Menachery, V.D., Yount, B.L., Jr., Debbink, K., Agnihothram, S., Gralinski, L.E., Plante, J.A., Graham, R.L., Scobey, T., Ge, X.Y., Donaldson, E.F., et al. (2015). A SARS-like cluster of circulating bat coronaviruses shows potential for human emergence. Nat. Med. *21*, 1508–1513.

Menachery, V.D., Yount, B.L., Jr., Sims, A.C., Debbink, K., Agnihothram, S.S., Gralinski, L.E., Graham, R.L., Scobey, T., Plante, J.A., Royal, S.R., et al. (2016). SARS-like WIV1-CoV poised for human emergence. Proc. Natl. Acad. Sci. USA *113*, 3048–3053.

Mercado, N.B., Zahn, R., Wegmann, F., Loos, C., Chandrashekar, A., Yu, J., Liu, J., Peter, L., McMahan, K., Tostanoski, L.H., et al. (2020). Single-shot Ad26 vaccine protects against SARS-CoV-2 in rhesus macaques. Nature *586*, 583–588.

Millet, J.K., and Whittaker, G.R. (2016). Murine Leukemia Virus (MLV)-based Coronavirus Spike-pseudotyped Particle Production and Infection. Bio. Protoc. *6*, e2035.

Otwinowski, J., McCandlish, D.M., and Plotkin, J.B. (2018). Inferring the shape of global epistasis. Proc. Natl. Acad. Sci. USA *115*, E7550–E7558.

Pallesen, J., Wang, N., Corbett, K.S., Wrapp, D., Kirchdoerfer, R.N., Turner, H.L., Cottrell, C.A., Becker, M.M., Wang, L., Shi, W., et al. (2017). Immunogenicity and structures of a rationally designed prefusion MERS-CoV spike antigen. Proc. Natl. Acad. Sci. USA *114*, E7348–E7357.

Piccoli, L., Park, Y.J., Tortorici, M.A., Czudnochowski, N., Walls, A.C., Beltramello, M., Silacci-Fregni, C., Pinto, D., Rosen, L.E., Bowen, J.E., et al. (2020). Mapping Neutralizing and Immunodominant Sites on the SARS-CoV-2 Spike Receptor-Binding Domain by Structure-Guided High-Resolution Serology. Cell *183*, 1024–1042.e21.

Pinto, D., Park, Y.J., Beltramello, M., Walls, A.C., Tortorici, M.A., Bianchi, S., Jaconi, S., Culap, K., Zatta, F., De Marco, A., et al. (2020). Cross-neutralization of SARS-CoV-2 by a human monoclonal SARS-CoV antibody. Nature *583*, 290–295.

Pinto, D., Sauer, M.M., Czudnochowski, N., Low, J.S., Alejandra Tortorici, M., Housley, M.P., Noack, J., Walls, A.C., Bowen, J.E., Guarino, B., et al. (2021). Broad betacoronavirus neutralization by a stem helix-specific human antibody. Science *373*, 1109–1116.

Plante, J.A., Liu, Y., Liu, J., Xia, H., Johnson, B.A., Lokugamage, K.G., Zhang, X., Muruato, A.E., Zou, J., Fontes-Garfias, C.R., et al. (2020). Spike mutation D614G alters SARS-CoV-2 fitness. Nature *592*, 116–121.

Polack, F.P., Thomas, S.J., Kitchin, N., Absalon, J., Gurtman, A., Lockhart, S., Perez, J.L., Pérez Marc, G., Moreira, E.D., Zerbini, C., et al.; C4591001 Clinical Trial Group (2020). Safety and Efficacy of the BNT162b2 mRNA Covid-19 Vaccine. N. Engl. J. Med. *383*, 2603–2615.

Rappazzo, C.G., Tse, L.V., Kaku, C.I., Wrapp, D., Sakharkar, M., Huang, D., Deveau, L.M., Yockachonis, T.J., Herbert, A.S., Battles, M.B., et al. (2021). Broad and potent activity against SARS-like viruses by an engineered human monoclonal antibody. Science *371*, 823–829.

Roberts, A., Deming, D., Paddock, C.D., Cheng, A., Yount, B., Vogel, L., Herman, B.D., Sheahan, T., Heise, M., Genrich, G.L., et al. (2007). A mouse-adapted SARS-coronavirus causes disease and mortality in BALB/c mice. PLoS Pathog. *3*, e5.

Rockx, B., Corti, D., Donaldson, E., Sheahan, T., Stadler, K., Lanzavecchia, A., and Baric, R. (2008). Structural basis for potent cross-neutralizing human monoclonal antibody protection against lethal human and zoonotic severe acute respiratory syndrome coronavirus challenge. J. Virol. *82*, 3220–3235.

Rogers, T.F., Zhao, F., Huang, D., Beutler, N., Burns, A., He, W.T., Limbo, O., Smith, C., Song, G., Woehl, J., et al. (2020). Isolation of potent SARS-CoV-2 neutralizing antibodies and protection from disease in a small animal model. Science *369*, 956–963.

Sauer, M.M., Tortorici, M.A., Park, Y.-J., Walls, A.C., Homad, L., Acton, O.J., Bowen, J.E., Wang, C., Xiong, X., de van der Schueren, W., et al. (2021). Structural basis for broad coronavirus neutralization. Nat. Struct. Mol. Biol. *28*, 478–486.

Shang, J., Ye, G., Shi, K., Wan, Y., Luo, C., Aihara, H., Geng, Q., Auerbach, A., and Li, F. (2020). Structural basis of receptor recognition by SARS-CoV-2. Nature *581*, 221–224.

Stamatatos, L., Czartoski, J., Wan, Y.-H., Homad, L.J., Rubin, V., Glantz, H., Neradilek, M., Seydoux, E., Jennewein, M.F., MacCamy, A.J., et al. (2021). mRNA vaccination boosts cross-variant neutralizing antibodies elicited by SARS-CoV-2 infection. Science, eabg9175. Published online March 25, 2021.

Starr, T.N., Greaney, A.J., Hilton, S.K., Ellis, D., Crawford, K.H.D., Dingens, A.S., Navarro, M.J., Bowen, J.E., Tortorici, M.A., Walls, A.C., et al. (2020a). Deep Mutational Scanning of SARS-CoV-2 Receptor Binding Domain Reveals Constraints on Folding and ACE2 Binding. Cell *182*, 1295–1310.e20.

Starr, T.N., Greaney, A.J., Addetia, A., Hannon, W.W., Choudhary, M.C., Dingens, A.S., Li, J.Z., and Bloom, J.D. (2020b). Prospective mapping of viral mutations that escape antibodies used to treat COVID-19. bioRxiv.

Starr, T.N., Czudnochowski, N., Liu, Z., Zatta, F., Park, Y.-J., Addetia, A., Pinto, D., Beltramello, M., Hernandez, P., Greaney, A.J., et al. (2021). SARS-CoV-2 RBD antibodies that maximize breadth and resistance to escape. Nature *597*, 97–102.

Suryadevara, N., Shrihari, S., Gilchuk, P., VanBlargan, L.A., Binshtein, E., Zost, S.J., Nargi, R.S., Sutton, R.E., Winkler, E.S., Chen, E.C., et al. (2021). Neutralizing and protective human monoclonal antibodies recognizing the N-terminal domain of the SARS-CoV-2 spike protein. Cell *184*, 2316–2331.e15.

Tegally, H., Wilkinson, E., Giovanetti, M., Iranzadeh, A., Fonseca, V., Giandhari, J., Doolabh, D., Pillay, S., San, E.J., Msomi, N., et al. (2020). Emergence and rapid spread of a new severe acute respiratory syndrome-related coronavirus 2 (SARS-CoV-2) lineage with multiple spike mutations in South Africa. medRxiv. https://doi.org/10.1101/2020.12.21.20248640.

ter Meulen, J., van den Brin, E.N., Poon, L.L.M., Marissen, W.E., Leung, C.S.W., Cox, F., Cheung, C..y., Bakker, A.Q., Bogaards, J.A., Deventer, E.V., et al. (2006). Human Monoclonal Antibody Combination against SARS Coronavirus: Synergy and Coverage of Escape Mutants. Plos Medicine *3*, e237.

Thomson, E.C., Rosen, L.E., Shepherd, J.G., Spreafico, R., da Silva Filipe, A., Wojcechowskyj, J.A., Davis, C., Piccoli, L., Pascall, D.J., Dillen, J., et al.; ISARIC4C Investigators; COVID-19 Genomics UK (COG-UK) Consortium (2021). Circulating SARS-CoV-2 spike N439K variants maintain fitness while evading antibody-mediated immunity. Cell *184*, 1171–1187.e20.

Tortorici, M.A., and Veesler, D. (2019). Structural insights into coronavirus entry. Adv. Virus Res. *105*, 93–116.

Tortorici, M.A., Beltramello, M., Lempp, F.A., Pinto, D., Dang, H.V., Rosen, L.E., McCallum, M., Bowen, J., Minola, A., Jaconi, S., et al. (2020). Ultrapotent human antibodies protect against SARS-CoV-2 challenge via multiple mechanisms. Science *370*, 950–957.

Tortorici, M.A., Czudnochowski, N., Starr, T.N., Marzi, R., Walls, A.C., Zatta, F., Bowen, J.E., Jaconi, S., Di Iulio, J., Wang, Z., et al. (2021). Broad sarbecovirus neutralization by a human monoclonal antibody. Nature *597*, 103–108.

Tostanoski, L.H., Wegmann, F., Martinot, A.J., Loos, C., McMahan, K., Mercado, N.B., Yu, J., Chan, C.N., Bondoc, S., Starke, C.E., et al. (2020). Ad26 vaccine protects against SARS-CoV-2 severe clinical disease in hamsters. Nat. Med. *26*, 1694–1700.

Walls, A.C., Tortorici, M.A., Bosch, B.J., Frenz, B., Rottier, P.J.M., DiMaio, F., Rey, F.A., and Veesler, D. (2016). Cryo-electron microscopy structure of a coronavirus spike glycoprotein trimer. Nature *531*, 114–117.

Walls, A.C., Xiong, X., Park, Y.J., Tortorici, M.A., Snijder, J., Quispe, J., Cameroni, E., Gopal, R., Dai, M., Lanzavecchia, A., et al. (2019). Unexpected Receptor Functional Mimicry Elucidates Activation of Coronavirus Fusion. Cell *176*, 1026–1039.e15.

Walls, A.C., Park, Y.J., Tortorici, M.A., Wall, A., McGuire, A.T., and Veesler, D. (2020a). Structure, Function, and Antigenicity of the SARS-CoV-2 Spike Glycoprotein. Cell *181*, 281–292.e6.

Walls, A.C., Fiala, B., Schäfer, A., Wrenn, S., Pham, M.N., Murphy, M., Tse, L.V., Shehata, L., O'Connor, M.A., Chen, C., et al. (2020b). Elicitation of Potent Neutralizing Antibody Responses by Designed Protein Nanoparticle Vaccines for SARS-CoV-2. Cell *183*, 1367–1382.e17.

Wang, Q., Zhang, Y., Wu, L., Niu, S., Song, C., Zhang, Z., Lu, G., Qiao, C., Hu, Y., Yuen, K.Y., et al. (2020). Structural and Functional Basis of SARS-CoV-2 Entry by Using Human ACE2. Cell *181*, 894–904.e9.

Wang, P., Nair, M.S., Liu, L., Iketani, S., Luo, Y., Guo, Y., Wang, M., Yu, J., Zhang, B., Kwong, P.D., et al. (2021a). Antibody resistance of SARS-CoV-2 variants B.1.351 and B.1.1.7. Nature *593*, 130–135.

Wang, P., Liu, L., Iketani, S., Luo, Y., Guo, Y., Wang, M., Yu, J., Zhang, B., Kwong, P.D., Graham, B.S., et al. (2021b). Increased resistance of SARS-CoV-2 variants B.I.35l and B.I.I.7. to antibody neutralization. bioRxiv. https://doi.org/10.1101/2021.01.25.428137.

Wang, Z., Schmidt, F., Weisblum, Y., Muecksch, F., Barnes, C.O., Finkin, S., Schaefer-Babajew, D., Cipolla, M., Gaebler, C., Lieberman, J.A., et al. (2021c). mRNA vaccine-elicited antibodies to SARS-CoV-2 and circulating variants. Nature *592*, 616–622.

Wec, A.Z., Wrapp, D., Herbert, A.S., Maurer, D.P., Haslwanter, D., Sakharkar, M., Jangra, R.K., Dieterle, M.E., Lilov, A., Huang, D., et al. (2020). Broad neutralization of SARS-related viruses by human monoclonal antibodies. Science *369*, 731–736.

Weisblum, Y., Schmidt, F., Zhang, F., DaSilva, J., Poston, D., Lorenzi, J.C.C., Muecksch, F., Rutkowska, M., Hoffmann, H.-H., Michailidis, E., et al. (2020). Escape from neutralizing antibodies by SARS-CoV-2 spike protein variants. eLife *9*, e61312.

Wibmer, C.K., Ayres, F., Hermanus, T., Madzivhandila, M., Kgagudi, P., Oosthuysen, B., Lambson, B.E., de Oliveira, T., Vermeulen, M., van der Berg, K., et al. (2021). SARS-CoV-2 501Y.V2 escapes neutralization by South African COVID-19 donor plasma. Nat. Med. *27*, 622–625.

Wrapp, D., Wang, N., Corbett, K.S., Goldsmith, J.A., Hsieh, C.L., Abiona, O., Graham, B.S., and McLellan, J.S. (2020). Cryo-EM structure of the 2019-nCoV spike in the prefusion conformation. Science *367*, 1260–1263.

Wu, K., Werner, A.P., Koch, M., Choi, A., Narayanan, E., Stewart-Jones, G.B.E., Colpitts, T., Bennett, H., Boyoglu-Barnum, S., Shi, W., et al. (2021). Serum Neutralizing Activity Elicited by mRNA-1273 Vaccine - Preliminary Report. N. Engl. J. Med. *384*, 1468–1470.

Yan, R., Zhang, Y., Li, Y., Xia, L., Guo, Y., and Zhou, Q. (2020). Structural basis for the recognition of SARS-CoV-2 by full-length human ACE2. Science *367*, 1444–1448.

Yu, J., Tostanoski, L.H., Peter, L., Mercado, N.B., McMahan, K., Mahrokhian, S.H., Nkolola, J.P., Liu, J., Li, Z., Chandrashekar, A., et al. (2020). DNA vaccine protection against SARS-CoV-2 in rhesus macaques. Science *369*, 806–811.

Yuan, M., Wu, N.C., Zhu, X., Lee, C.D., So, R.T.Y., Lv, H., Mok, C.K.P., and Wilson, I.A. (2020). A highly conserved cryptic epitope in the receptor binding domains of SARS-CoV-2 and SARS-CoV. Science *368*, 630–633.

Yurkovetskiy, L., Wang, X., Pascal, K.E., Tomkins-Tinch, C., Nyalile, T.P., Wang, Y., Baum, A., Diehl, W.E., Dauphin, A., Carbone, C., et al. (2020). Structural and Functional Analysis of the D614G SARS-CoV-2 Spike Protein Variant. Cell *183*, 739–751.e8.

Zhou, H., Chen, X., Hu, T., Li, J., Song, H., Liu, Y., Wang, P., Liu, D., Yang, J., Holmes, E.C., et al. (2020a). A Novel Bat Coronavirus Closely Related to SARS-CoV-2 Contains Natural Insertions at the S1/S2 Cleavage Site of the Spike Protein. Curr. Biol. *30*, 2196–2203.e3.

Zhou, P., Yang, X.L., Wang, X.G., Hu, B., Zhang, L., Zhang, W., Si, H.R., Zhu, Y., Li, B., Huang, C.L., et al. (2020b). A pneumonia outbreak associated with a new coronavirus of probable bat origin. Nature *579*, 270–273.

Zost, S.J., Gilchuk, P., Case, J.B., Binshtein, E., Chen, R.E., Nkolola, J.P., Schäfer, A., Reidy, J.X., Trivette, A., Nargi, R.S., et al. (2020). Potently neutralizing and protective human antibodies against SARS-CoV-2. Nature *584*, 443–449.

STAR★METHODS

KEY RESOURCES TABLE

REAGENT or RESOURCE	SOURCE	IDENTIFIER
Antibodies		
CR3022	ter Meulen et al., 2006	N/A
S309	Pinto et al., 2020	N/A
S2X259	Tortorici et al., 2021	N/A
S2H14	Piccoli et al., 2020	N/A
S230	Rockx et al., 2008	N/A
Goat anti-mouse HRP	Invitrogen	Cat #626520; Lot #TG275230; AB_2533947
Goat anti-human HRP	Invitrogen	Cat #A18817; Lot #65-180-071919; AB_2535594
Streptavidin-HRP	Thermo Scientific	Cat #N100
CD45/LCA-A700-C61	BD Biosciences	Cat#5605010
CD11c-BV501	Biolegend	Cat#117338; AB_2562016
SiglecF-BV650	BD Biosceinces	Cat#740557; AB_2740258
I1-Hybridoma	ATCC	CRL-2700
Biological samples		
BALB/c mice	Jackson Laboratory	Cat#000651
Pigtail macaques (Macaca nemestrina)	WANPRC	
Rhesus macaques (Macaca mulatta)	NIRC	
20/130 COVID-19 plasma	NIBSC	Sample#20/130
VSV (G*ΔG-luciferase)	Kaname et al., 2010	N/A
Chemicals, peptides, and recombinant proteins		
AddaVax adjuvant	InvivoGen	Cat# vac-adx-10
AS03	GSK	N/A
O/W	VFI	N/A
TMB	SeraCare	Cat# 5120-0083
Thrombin	Sigma	Cat# T9326-150UN
Immobilized Papain	ThermoScientific	Cat# 20341
LysC-endoproteinase	NEB	Cat# P8109S
EZ-Link Sulfo-NHS-LC Biotinylation Kit	Thermo Fisher Scientific	Cat#21435
Experimental models: Cell lines		
Expi 293F	ThermoFisher	Cat #A14527
HEK-ACE2 adherent	BEI (Gift from Bloom lab)	Sample#NR-52511
HEK293T/17 Adherent	ATCC	Cat# CRL-11268
Recombinant DNA		
HexaPro S	Hsieh et al., 2020	N/A
RBD-16GS-50A	GenScript Walls et al., 2020b	N/A
RBD-12GS-50A	GenScript Walls et al., 2020b	N/A
SARS-COV-RBD-16GS-50A	GenScript	N/A
WIV1-RBD-16GS-50A	GenScript	N/A
RaTG13-RBD-16GS-50A	GenScript	N/A
SARS-CoV-2 S-2P trimer	GenScript Walls et al., 2020a	Vector# BEI NR-52421
SARS-CoV S-2P trimer	GeneArt Walls et al., 2019	N/A
SARS-CoV-2 RBD	GenScript Walls et al., 2020a	Vector# BEI NR-52422
SARS-CoV RBD	GenScript	N/A

(*Continued on next page*)

Continued

REAGENT or RESOURCE	SOURCE	IDENTIFIER
WIV1 RBD	GenScript	N/A
RaTG13 RBD	GenScript	N/A/
SARS-CoV-2 S full-length D614G (YP 009724390.1)	Crawford et al., 2020	Vector# BEI NR-52514
SHC014 S full-length (AGZ48806.1)	GenScript	N/A
SARS-CoV S full-length (YP 009825051.1)	GeneArt (Walls et al., 2020)	N/A
RaTG13 S full-length (QHR63300.2)	GenScript	N/A
WIV1 full-length S (AGZ48831.1)	GenScript	N/A
PangolinGD full-length S (QLR06867.1)	GenScript	N/A
Murine leukemia virus gag-pol	Millet and Whittaker 2016	N/A
pTG-Luciferase	Millet and Whittaker 2016	N/A
HIV Hgpm2	Crawford et al., 2020	Vector# BEI NR-52517
HIV luciferase	Crawford et al., 2020	Vector# BEI NR-52516
HIV tat1b	Crawford et al., 2020	Vector# BEI NR-52518
HIV Rev1b	Crawford et al., 2020	Vector# BEI NR-52519
Software and algorithms		
UCSF ChimeraX	Goddard et al., 2018	https://www.rbvi.ucsf.edu/chimerax/
Prism	Graphpad	https://www.graphpad.com/scientific-software/prism/
FlowJo v10	FlowJo	https://www.flowjo.com
Dms-variants package	Greaney et al., 2020	https://jbloomlab.github.io/dms_variants/dms_variants.globalepistasis.html
Other		
Octet Biosensors: protein A	Sartorius (FortéBio)	Cat# 18-5010
Octet Biosensors: ARG2	Sartorius (FortéBio)	Cat# 18-5092
EM supplies 300 mesh grids	Ted Pella	Cat# 01843-F
Filter paper	Cytiva	Cat# 1004047
Uranyl formate	SPI Chem	Cat# 02545-AA
Unis Capillary Cassettes	Unchained Labs	Cat# 201-1010
PrismA Protein A resin	Cytiva	Cat# 17549802
Superdex 200 Increase SEC column	Cytiva	Cat# 28-9909-44
Superose 6 Increase SEC column	Cytiva	Cat# 29091596
Talon resin	TaKaRa	Cat# 635652
Excel resin	Cytiva	Cat# 17371203
Patterson Veterinary, Isoflurane, USP	Patterson	Cat# 07-893-1389
EndoSafe LAL Test Cartridges	Charles River Labs	Cat # PTS20005F
Lemo21(DE3)	New England BioLabs	Cat#C2528J
Isopropyl-B-D-thiogalactoside (IPTG)	Sigma Aldrich	Cat#I6758
Kanamycin Sulfate	Sigma-Aldrich	Cat#K1876
HiLoad S200 pg	Cytiva	Cat#28989336
Ni Sepharose 6 FF	Cytiva	Cat#17531808
HisTrap FF	Cytiva	Cat#17525501

RESOURCE AVAILABILITY

Lead contact

Further information and requests for resources and reagents should be directed to and will be fulfilled by the Lead Contact, David Veesler (dveesler@uw.edu).

Materials availability

All reagents will be made available on request after completion of a Materials Transfer Agreement.

Data and code availability

All data supporting the findings of this study are found within the paper and its Supplemental information, and are available from the Lead Contact author upon request. Additional supplemental items are available from Mendeley Data at https://doi.org/10.17632/5k989kb8t7.1.

EXPERIMENTAL MODEL AND SUBJECT DETAILS

Cell lines

Expi293F (derived from 293 cells which are female) cells are derived from the HEK293F cell line (Life Technologies). Expi293F cells were grown in Expi293 Expression Medium (Life Technologies), cultured at 36.5°C with 8% CO_2 and shaking at 150 rpm. HEK293T/17 is a female human embryonic kidney cell line (ATCC). The HEK-ACE2 (derived from HEK293T cells which are female) adherent cell line was obtained through BEI Resources, NIAID, NIH: Human Embryonic Kidney Cells (HEK293T) Expressing Human Angiotensin-Converting Enzyme 2, HEK293T-hACE2 Cell Line, NR-52511. All adherent cells were cultured at 37°C with 8% CO_2 in flasks with DMEM + 10% FBS (Hyclone) + 1% penicillin-streptomycin. Cell lines other than Expi293F were not tested for mycoplasma contamination nor authenticated.

Mice

Female BALB/c mice (Stock # 000651, BALB/c cByJ mice) four weeks old were obtained from Jackson Laboratory, Bar Harbor, Maine, and maintained at the Comparative Medicine Facility at the University of Washington, Seattle, WA, accredited by the American Association for the Accreditation of Laboratory Animal Care International (AAALAC). Animal procedures were performed under the approvals of the Institutional Animal Care and Use Committee (IACUC) of University of Washington, Seattle, WA, and University of North Carolina, Chapel Hill, NC.

Pigtail macaques

Two adult male Pigtail macaques (*Macaca nemestrina*) were immunized in this study. All animals were housed at the Washington National Primate Research Center (WaNPRC), an AAALAC International accredited institution. All experiments were approved by The University of Washington's IACUC. Animals were singly housed in comfortable, clean, adequately-sized cages with ambient temperatures between 72–82°F. Animals received environmental enrichment for the duration of the study including grooming contact, perches, toys, foraging experiences and access to additional environment enrichment devices. Water was available through automatic watering devices and animals were fed a commercial monkey chow, supplemented daily with fruits and vegetables. Throughout the study, animals were checked twice daily by husbandry staff.

Rhesus macaques

Male Rhesus macaques (Macaca mulatta) of Indian origin, aged 3–7 years were assigned to the study (Arunachalam et al., 2021). Animals were distributed between the groups such that the age and weight distribution were comparable across the groups. Animals were housed and maintained at the New Iberia Research Center (NIRC) of the University of Louisiana at Lafayette, an AAALAC International accredited institution, in accordance with the rules and regulations of the Guide for the Care and Use of Laboratory Animal Resources. The entire study (protocol 2020-8808-15) was reviewed and approved by the University of Louisiana at Lafayette IACUC. All animals were negative for SIV, simian T cell leukemia virus, and simian retrovirus.

Convalescent human sera

Samples collected between 1–60 days post infection from individuals who tested positive for SARS-CoV-2 by PCR were profiled for anti-SARS-CoV-2 S antibody responses and those with anti-S Ab responses were maintained in the cohort (Walls et al., 2020b). Individuals were enrolled as part of the HAARVI study at the University of Washington in Seattle, WA. Baseline sociodemographic and clinical data for these individuals are summarized in Table S1. This study was approved by the University of Washington Human Subjects Division Institutional Review Board (STUDY00000959 and STUDY00003376). All experiments were performed in at least two replicates. One sample is the 20/130 COVID-19 plasma from NIBSC (https://www.nibsc.org/documents/ifu/20-130.pdf).

Pfizer vaccinated human sera

Blood samples were collected from participants who had received both doses of the Pfizer mRNA vaccine and were 7–30 days post second vaccine dose. Clinical data for these individuals are summarized in Table S1. Individuals were enrolled in the UWARN: COVID-19 in WA study at the University of Washington in Seattle, WA. This study was approved by the University of Washington Human Subjects Division Institutional Review Board (STUDY00010350).

METHOD DETAILS

Plasmid construction

The SARS-CoV-2-RBD-Avi construct was synthesized by GenScript into pcDNA3.1- with an N-terminal mu-phosphatase signal peptide and a C-terminal octa-histidine tag, flexible linker, and avi tag (GHHHHHHHHGGSSGLNDIFEAQKIEWHE). The boundaries of the construct are N-$_{328}$RFPN$_{331}$ and $_{528}$KKST$_{531}$-C (Walls et al., 2020a). The GD-Pangolin (326-527), WIV1 (316-518), RaTG13 (359-562), RmYN02 (307-492), and ZXC21 (323-507) were synthesized by GenScript into vector pcDNA3.1- or CMVR with a preceding mu-phosphatase signal peptide and a C-terminal octahistidine tag. SARS-CoV-1 (306-575) was subcloned from a GenArt synthesized SARS-CoV-1 Spike ectodomain. The SARS-CoV S2P ((Pallesen et al., 2017)) was synthesized by GeneArt and placed into a modified pOPING vector with its original N-terminal mu-phosphatase signal peptide, and an engineered C-terminal extension: SG-RENLYFQG (TEV protease site), GGGSG-YIPEAPRDGQAYVRKDGEWVLLSTFL (foldon trimerization motif), G-HHHHHH (hexa-histidine tag), just upstream of the predicted transmembrane region (YIK). The SARS-CoV-2 S2P ectodomain trimer (GenBank: YP_009724390.1, BEI NR-52420) was synthesized by GenScript into pCMV with an N-terminal mu-phosphatase signal peptide and a C-terminal TEV cleavage site (GSGRENLYPQG), T4 fibritin foldon (GGGSGYIPEAPRDGQAYVRKDGEWVLLSTPL), and octa-histidine tag (GHHHHHHHH) (Walls et al., 2020a). The construct contains the 2P mutations (proline substitutions at residues 986 and 987; and an $_{682}$SGAG$_{685}$ substitution at the furin cleavage site. The SARS-CoV-2 RBD was genetically fused to the N terminus of the trimeric I53-50A nanoparticle component using 12 or 16 glycine and serine residues. RBD-12GS-I53-50A fusions were synthesized and cloned by Genscript into pCMV. The RBD-16GS-I53-50A fusion was cloned into pCMV/R using the Xba1 and AvrII restriction sites and Gibson assembly (Gibson et al., 2009). All RBD-bearing components contained an N-terminal mu-phosphatase signal peptide and a C-terminal octa-histidine tag. Human ACE2 ectodomain was genetically fused to a sequence encoding a thrombin cleavage site and a human Fc fragment at the C-terminal end. hACE2-Fc was synthesized and cloned by GenScript with a BM40 signal peptide. Genes encoding CR3022 heavy and light chains were ordered from GenScript and cloned into pCMV/R. S309 construct as previously described (Pinto et al., 2020). SARS-CoV-2 HexaPro construct is as previously described (Hsieh et al., 2020) and placed into CMVR with an octa-his tag.

Transient transfection

Proteins were produced using endotoxin free DNA in Expi293F cells grown in suspension using Expi293F expression medium (Life Technologies) at 33°C, 70% humidity, 8% CO_2 rotating at 150 rpm. The cultures were transfected using PEI-MAX (Polyscience) with cells grown to a density of 3.0 million cells per mL and cultivated for 3 days. Supernatants were clarified by centrifugation (5 min at 4000 *rcf.*), addition of PDADMAC solution to a final concentration of 0.0375% (Sigma Aldrich, #409014), and a second spin (5 min at 4000 *rcf.*).

Microbial protein expression and purification

The I53-50A and I53-50B.4.PT1 proteins (Bale et al., 2016) were expressed in Lemo21(DE3) (NEB) in LB (10 g Tryptone, 5 g Yeast Extract, 10 g NaCl) grown in 2 L baffled shake flasks or a 10 L BioFlo 320 Fermenter (Eppendorf). Cells were grown at 37°C to an OD600 ~0.8, and then induced with 1 mM IPTG. Expression temperature was reduced to 18°C and the cells shaken for ~16 h. The cells were harvested and lysed by microfluidization using a Microfluidics M110P at 18,000 psi in 50 mM Tris, 500 mM NaCl, 30 mM imidazole, 1 mM PMSF, 0.75% CHAPS. Lysates were clarified by centrifugation at 24,000 g for 30 min and applied to a 2.6 × 10 cm Ni Sepharose 6 FF column (Cytiva) for purification by IMAC on an AKTA Avant150 FPLC system (Cytiva). Protein of interest was eluted over a linear gradient of 30 mM to 500 mM imidazole in a background of 50 mM Tris pH 8, 500 mM NaCl, 0.75% CHAPS buffer. Peak fractions were pooled, concentrated in 10K MWCO centrifugal filters (Millipore), sterile filtered (0.22 μm) and applied to either a Superdex 200 Increase 10/300, or HiLoad S200 pg GL SEC column (Cytiva) using 50 mM Tris pH 8, 500 mM NaCl, 0.75% CHAPS buffer. I53-50A elutes at ~0.6 column volume (CV). I53-50B.4PT1 elutes at ~0.45 CV. After sizing, bacterial-derived components were tested to confirm low levels of endotoxin before using for nanoparticle assembly.

Protein purification

Proteins containing His tags were purified from clarified supernatants via a batch bind method where each clarified supernatant was supplemented with 1 M Tris-HCl pH 8.0 to a final concentration of 45 mM and 5 M NaCl to a final concentration of ~310 mM. Talon cobalt affinity resin (Takara) was added to the treated supernatants and allowed to incubate for 15 min with gentle shaking. Resin was collected using vacuum filtration with a 0.2 μm filter and transferred to a gravity column. The resin was washed with 20 mM Tris pH 8.0, 300 mM NaCl, and the protein was eluted with 3 column volumes of 20 mM Tris pH 8.0, 300 mM NaCl, 300 mM imidazole. The batch bind process was then repeated and the first and second elutions combined. SDS-PAGE was used to assess purity. RBD-I53-50A fusion protein IMAC elutions were concentrated to > 1 mg/mL and subjected to three rounds of dialysis into 50 mM Tris pH 7.4, 185 mM NaCl, 100 mM Arginine, 4.5% glycerol, and 0.75% w/v 3-[(3-cholamidopropyl)dimethylammonio]-1-propanesulfonate (CHAPS) in a hydrated 10K molecular weight cutoff dialysis cassette (Thermo Scientific). S2P and HexaPro IMAC elution fractions were concentrated to ~1 mg/mL and dialyzed three times into 50 mM Tris pH 8, 150 mM NaCl, 0.25% L-Histidine in a hydrated 10K molecular weight cutoff dialysis cassette (Thermo Scientific).

Clarified supernatants of cells expressing monoclonal antibodies and human ACE2-Fc were purified using a MabSelect PrismA 2.6 × 5 cm column (Cytiva) on an AKTA Avant150 FPLC (Cytiva). Bound antibodies were washed with five column volumes of 20 mM $NaPO_4$, 150 mM NaCl pH 7.2, then five column volumes of 20 mM $NaPO_4$, 1 M NaCl pH 7.4 and eluted with three column volumes of 100 mM glycine at pH 3.0. The eluate was neutralized with 2 M Trizma base to 50 mM final concentration. SDS-PAGE was used to assess purity.

Recombinant S309 was expressed as a Fab in expiCHO cells transiently co-transfected with plasmids expressing the heavy and light chain, as described above (see Transient transfection) (Pinto et al., 2020). The protein was affinity-purified using a HiTrap Protein A Mab select Xtra column (Cytiva) followed by desalting against 20 mM $NaPO_4$, 150 mM NaCl pH 7.2 using a HiTrap Fast desalting column (Cytiva). The protein was sterilized with a 0.22 μm filter and stored at 4°C until use.

In vitro nanoparticle assembly and purification

Total protein concentration of purified individual nanoparticle components was determined by measuring absorbance at 280 nm using a UV/vis spectrophotometer (Agilent Cary 8454) and calculated extinction coefficients. The assembly steps were performed at room temperature with addition in the following order: RBD-I53-50A trimeric fusion protein, followed by additional buffer (50 mM Tris pH 7.4, 185 mM NaCl, 100 mM Arginine, 4.5% glycerol, and 0.75% w/v CHAPS) as needed to achieve desired final concentration, and finally I53-50B.4PT1 pentameric component (in 50 mM Tris pH 8, 500 mM NaCl, 0.75% w/v CHAPS), with a molar ratio of RBD-I53-50A:I53-50B.4PT1 of 1.1:1. All RBD-I53-50 *in vitro* assemblies were incubated at 2-8°C with gentle rocking for at least 30 min before subsequent purification by SEC in order to remove residual unassembled component. Different columns were utilized depending on purpose: Superose 6 Increase 10/300 GL column was used analytically for nanoparticle size estimation, a Superdex 200 Increase 10/300 GL column used for small-scale pilot assemblies, and a HiLoad 26/600 Superdex 200 pg column used for nanoparticle production. Assembled particles were purified in 50 mM Tris pH 7.4, 185 mM NaCl, 100 mM Arginine, 4.5% glycerol, and 0.75% w/v CHAPS, and elute at ~11 mL on the Superose 6 column and in the void volume of Superdex 200 columns. Assembled nanoparticles were sterile filtered (0.22 μm) immediately prior to column application and following pooling of fractions.

Endotoxin measurements

Endotoxin levels in protein samples were measured using the EndoSafe Nexgen-MCS System (Charles River). Samples were diluted 1:50 or 1:100 in Endotoxin-free LAL reagent water, and applied into wells of an EndoSafe LAL reagent cartridge. Charles River EndoScan-V software was used to analyze endotoxin content, automatically back-calculating for the dilution factor. Endotoxin values were reported as EU/mL which were then converted to EU/mg based on UV/vis measurements. Our threshold for samples suitable for immunization was < 50 EU/mg.

Pigtail macaque immunization

Two Pigtail macaques were immunized with 250 μg of RBD-12GS-I53-50 nanoparticle (88 μg RBD antigen) with AddaVax at day 0, day 28, and O/W at day 168. Blood was collected every 14 days post-prime. Blood was collected in serum collection tubes and allowed to clot at room temperature. Serum was isolated after a 15 min spin at 1455 x g for 15 min and stored at −80C until use. Prior to vaccination or blood collection, animals were sedated with an intramuscular injection (10 mg/kg) of ketamine (Ketaset®; Henry Schein). Prior to inoculation, immunogen suspensions were gently mixed 1:1 vol/vol with AddaVax adjuvant for immunizations 1 and 2 and O/W for immunization 3 (VFI) to reach a final concentration of 0.250 mg/mL antigen. The vaccine was delivered intramuscularly into both quadriceps muscles with 1 mL per injection site on days 0, 28, and 168. All injection sites were shaved prior to injection. Animals were observed daily for general health (activity and appetite, urine/feces output) and for evidence of reactogenicity at the vaccine inoculation site (swelling, erythema, and pruritus) for up to 1 week following vaccination. They also received physical exams including temperature and weight measurements at each study time point. None of the animals became severely ill during the course of the study nor required euthanasia.

Rhesus macaque immunization

Adapted from Arunachalam et al. (2021). AS03 was kindly provided by GSK Vaccines. AS03 is an oil-in-water emulsion that contains 11.86 mg a-tocopherol, 10.69 mg squalene, and 4.86 mg polysorbate 80 (Tween-80) in PBS. For each dose, RBD-NP was diluted to 50 μg/ml (RBD component) in 250 μL of Tris-buffered saline (TBS) and mixed with an equal volume of AS03.The dose of AS03 was 50% v/v (equivalent of one human dose). Soluble HexaPro was diluted to 50 μg/ml in 250 μL of Tris-buffered saline (TBS) and mixed with an equal volume of AS03. All immunizations were administered via the intramuscular route in right forelimbs. The volume of each dose was 0.5 ml.

Deep mutational scanning

All mutations that escape serum antibody binding were mapped via a deep mutational scanning approach (Greaney et al., 2020, 2021b). We used previously described yeast-display RBD mutant libraries (Greaney et al., 2020; Starr et al., 2020a). Briefly, duplicate mutant libraries were constructed in the spike receptor binding domain (RBD) from SARS-CoV-2 (isolate Wuhan-Hu-1, GenBank: MN908947, residues N331-T531) and contain 3,804 of the 3,819 possible amino-acid mutations, with > 95% present as single mutants. Each RBD variant was linked to a unique 16-nucleotide barcode sequence to facilitate downstream sequencing. As previously

described, libraries were sorted for RBD expression and ACE2 binding to eliminate RBD variants that are completely misfolded or non-functional (i.e., lacking modest ACE2 binding affinity) (Greaney et al., 2020).

Antibody escape mapping experiments were performed in biological duplicate using two independent mutant RBD libraries, with minor modifications from Greaney et al. (2020), and exactly as described in Greaney et al. (2021b). The antibody escape mapping for the vaccinated NHP serum was performed in this study; the antibody escape mapping from convalescent human plasma was performed in Greaney et al. (2021b). Briefly, mutant yeast libraries induced to express RBD were washed and incubated with plasma or serum at a range of dilutions for 1 h at room temperature with gentle agitation. For each sample, we chose a sub-saturating dilution such that the amount of fluorescent signal due to plasma antibody binding to RBD was approximately equal across samples. A 1:1000 dilution was used for the vaccinated NHP serum, and the exact dilutions of human convalescent plasma are reported in Greaney et al. (2021b). After the antibody incubations, the libraries were secondarily labeled with 1:100 FITC-conjugated anti-MYC antibody (Immunology Consultants Lab, CYMC-45F) to label for RBD expression and and 1:200 Alexa-647-conjugated goat anti-human-IgA+IgG+IgM (Jackson ImmunoResearch 109-605-064) to label for bound serum or plasma antibodies. A flow cytometric selection gate was drawn to capture approximately 5% of the RBD mutant libraries with the lowest amount of plasma binding for their degree of RBD expression. For each sample, approximately 10 million RBD+ cells were processed on the cytometer. Antibody-escaped cells were grown overnight in SD-CAA (6.7g/L Yeast Nitrogen Base, 5.0g/L Casamino acids, 1.065 g/L MES acid, and 2% w/v dextrose) to expand cells prior to plasmid extraction.

Plasmid samples were prepared from pre-selection and overnight cultures of antibody-escaped cells (Zymoprep Yeast Plasmid Miniprep II) as previously described (Greaney et al., 2020). The 16-nucleotide barcode sequences identifying each RBD variant were amplified by PCR and sequenced on an Illumina HiSeq 2500 with 50 bp single-end reads as described in Greaney et al. (2020 and Starr et al. (2020a).

Escape fractions were computed as described in Greaney et al. (2020), and exactly as described in Greaney et al. (2021b). We used the dms_variants package (https://jbloomlab.github.io/dms_variants/, version 0.8.2) to process Illumina sequences into counts of each barcoded RBD variant in each pre-sort and antibody-escape population using the barcode/RBD look-up table from Starr et al. (2021).

For each serum selection, we computed the ''escape fraction'' for each barcoded variant using the deep sequencing counts for each variant in the original and serum-escape populations and the total fraction of the library that escaped antibody binding via the formula provided in Greaney et al. (2020). These escape fractions represent the estimated fraction of cells expressing that specific variant that fall in the antibody escape bin, such that a value of 0 means the variant is always bound by serum and a value of 1 means that it always escapes serum binding. We then applied a computational filter to remove variants with low sequencing counts or highly deleterious mutations that might cause antibody escape simply by leading to poor expression of properly folded RBD on the yeast cell surface (Greaney et al., 2020; Starr et al., 2020a). Specifically, we removed variants that had (or contained mutations with) ACE2 binding scores < -2.35 or expression scores < -1, using the variant- and mutation-level deep mutational scanning scores from Starr et al. (2020a). Note that these filtering criteria are slightly more stringent than those used in Greaney et al. (2020) but are identical to those used in Greaney et al. (2021b) and Starr et al. (2020b).

We next deconvolved variant-level escape scores into escape fraction estimates for single mutations using global epistasis models (Otwinowski et al., 2018) implemented in the dms_variants package, as detailed at (https://jbloomlab.github.io/dms_variants/dms_variants.globalepistasis.html) and described in Greaney et al. (2020). The reported escape fractions throughout the paper are the average across the libraries (correlations shown in Figure S2); these scores are also in Table S1 and at https://github.com/jbloomlab/SARS-CoV-2-RBD_MAP_RBD-nano-vax-NHP1/blob/main/results/supp_data/NHP_HCS_raw_data.csv. Sites of strong escape from each antibody were determined heuristically as sites whose summed mutational escape scores were at least 10 times the median sitewise sum of selection, and within 10-fold of the sitewise sum of the most strongly selected site. Sites shown in Figures 2 and S2A are the sites of strong escape for any of the three human convalescent plasma, plus sites 417, 452, and 501 due to their prevalence in circulating SARS-CoV-2 variants. For each plasma, the y axis is scaled to be the greatest of (a) the maximum site-wise escape metric observed for that plasma, (b) 20x the median site-wise escape fraction observed across all sites for that plasma, or (c) an absolute value of 1.0 (to appropriately scale plasma that are not ''noisy'' but for which no mutation has a strong effect on plasma binding). Full documentation of the computational analysis is at https://github.com/jbloomlab/SARS-CoV-2-RBD_MAP_RBD-nano-vax-NHP1. These results are also available in a zoomable, interactive form at https://jbloomlab.github.io/SARS-CoV-2-RBD_MAP_RBD-nano-vax-NHP1/.

ELISA

For anti-S2P ELISA, 25 μL of 2 μg/mL S2P was plated onto 384-well Nunc Maxisorp (ThermoFisher) plates in PBS and sealed overnight at RT. The next day plates were washed 4 × in Tris Buffered Saline Tween (TBST) using a plate washer (BioTek) and blocked with SuperBlock (ThermoFisher) for 1 h at 37°C. Plates were washed 4 × in TBST and 1:5 serial dilutions of mouse, NHP, or human sera were made in 25 μL TBST and incubated at 37°C for 1 h. Plates were washed 4 × in TBST, then anti-mouse (Invitrogen), anti-NHP (AlphaDiagnostics), or anti-human (Invitrogen) horseradish peroxidase-conjugated antibodies were diluted 1:5,000 and 25 μL added to each well and incubated at 37°C for 1 h. Plates were washed 4 × in TBST and 25 μL of TMB (SeraCare) was added to every well for

~5 min at room temperature. The reaction was quenched with the addition of 25 μL of 1 N HCl. Plates were immediately read at 450 nm on a BioTek plate reader and data plotted and fit in Prism (GraphPad) using nonlinear regression sigmoidal, 4PL, X is log(concentration) to determine EC_{50} values from curve fits.

Competition ELISA of NHP sera with hACE2, CR3022 IgG, and S309 IgG for immobilized SARS-CoV-2 S2P

384-well Maxisorp plates (Thermo Fisher) were coated overnight at room temperature with 3 μg/mL of SARS-CoV-2 S2P (Pallesen et al., 2017) in 20mM Tris pH 8 and 150mM NaCl. Plates were slapped dry and blocked with Blocker Casein in TBS (Thermo Fisher) for one hour at 37°C. Plates were slapped dry and NHP sera was serially diluted 1:4 in TBST with an initial dilution of 1:4 for hACE2 competition or 1:2 for antibody competition. Random primary amine biotinylated (Thermo Fisher) hACE2-Fc, CR3022 (Yuan et al., 2020), or S309 (Pinto et al., 2020) were added, bringing the concentration of each well to the EC_{50} values of 0.2nM, 2nm, and 0.01nM, respectively. Plates were left for one hour at 37°C, then washed 4x with TBST using a 405 TS Microplate Washer (BioTek) followed by addition of 1:500 streptavidin-HRP (Thermo Fisher) for one hour at 37°C. Plates were washed 4x and TMB Microwell Peroxidase (Seracare) was added. The reaction was quenched after 1-2 minutes with 1 N HCl and the A450 of each well was read using a BioTek plate reader (BioTek). Data plotted and fit in Prism (GraphPad) using nonlinear regression sigmoidal, 4PL, X is log(concentration) to determine EC_{50} values from curve fits with upper and lower constraints determined by uncompeted ELISA per antigen.

Competition ELISA of mouse sera and immobilized hACE2 or mAbs with SARS-CoV-2 or SARS-CoV S2P

384-well Maxisorp plates (Thermo Fisher) were coated overnight at room temperature with 3 μg/mL of hACE2-Fc, CR3022 (Yuan et al., 2020), or S309 (Pinto et al., 2020) in 20mM Tris pH 8 and 150mM NaCl. Plates were slapped dry and blocked with Blocker Casein in TBS (Thermo Fisher) for one hour at 37°C. Plates were slapped dry and a 30-minute pre-incubated 1:5 serial dilution of mouse sera in TBST, with in initial dilution of 1:50 for hACE2-Fc competition or 1:10 for antibody competition, and a constant concentration of biotinylated (Avidity) SARS-CoV-2 S2P or SARS-CoV 2P at their EC_{50} values were added. Spike concentrations were 0.63nM, 5.98nM, and 0.22nM of SARS-CoV-2 S2P or 4.11nM, 2.89nM, and 0.19nM of SARS-CoV S2P for immobilized hACE2, CR3022, and S309, respectively. Plates were left for one hour at 37°C, then washed 4x with TBST using a 405 TS Microplate Washer (BioTek) followed by addition of 1:500 streptavidin-HRP (Thermo Fisher) for one hour at 37°C. Plates were washed 4x and TMB Microwell Peroxidase (Seracare) was added. The reaction was quenched after 1-2 minutes with 1 N HCl and the A450 of each well was read using a BioTek plate reader (BioTek). Data plotted and fit in Prism (GraphPad) using nonlinear regression sigmoidal, 4PL, X is log(concentration) to determine EC_{50} values from curve fits.

Pseudovirus production

MLV-based D614G SARS-CoV-2 S and SARS-CoV S pseudotypes were prepared as previously described (Millet and Whittaker, 2016; Walls et al., 2020a, 2020b). Briefly, HEK293T cells were co-transfected using Lipofectamine 2000 (Life Technologies) with an S-encoding plasmid, an MLV Gag-Pol packaging construct, and the MLV transfer vector encoding a luciferase reporter according to the manufacturer's instructions. Cells were washed 3 × with Opti-MEM and incubated for 5 h at 37°C with transfection medium. DMEM containing 10% FBS was added for 60 h. The supernatants were harvested by spinning at 2,500 g, filtered through a 0.45 μm filter, concentrated with a 100 kDa membrane for 10 min at 2,500 g and then aliquoted and stored at −80°C.

HIV-based pseudotypes were prepared as previously described (Crawford et al., 2020). Briefly, HEK293T cells were cotransfected using Lipofectamine 2000 (Life Technologies) with an S-encoding plasmid (D614G SARS-CoV-2 S (YP 009724390.1), Pangolin-Guangdong S (QLR06867.1), SARS-CoV S (YP 009825051.1), P1, B.1.351 S, B.1.1.7, and B.1.1.7+E484K S) an HIV Gag-Pol, Tat, Rev1B packaging construct, and the HIV transfer vector encoding a luciferase reporter according to the manufacturer's instructions. Cells were washed 3 × with Opti-MEM and incubated for 5 h at 37°C with transfection medium. DMEM containing 10% FBS was added for 60 h. The supernatants were harvested by spinning at 2,500 g, filtered through a 0.45 μm filter, concentrated with a 100 kDa membrane for 10 min at 2,500 g and then aliquoted and stored at −80°C.

D614G SARS-CoV-2 S (YP 009724390.1), D614G SARS-CoV-2 point mutants, SHC014 (AGZ48806.1), RaTG13 S (QHR63300.2), Pangolin-Guangdong S (QLR06867.1), SARS-CoV S (YP 009825051.1), WIV1 S (AGZ48831.1), B.1.351 S, P1, and B.1.1.7 S pseudotyped VSV viruses were prepared as described previously (McCallum et al., 2021a; Sauer et al., 2021). Briefly, 293T cells in DMEM supplemented with 10% FBS, 1% PenStrep seeded in 10-cm dishes were transfected with the plasmid encoding for the corresponding S glycoprotein using lipofectamine 2000 (Life Technologies) following manufacturer's indications. One day post-transfection, cells were infected with VSV(G*ΔG-luciferase) and after 2 h were washed five times with DMEM before adding medium supplemented with anti-VSV-G antibody (I1- mouse hybridoma supernatant, CRL- 2700, ATCC). Virus pseudotypes were harvested 18-24 h post-inoculation, clarified by centrifugation at 2,500 x g for 5 min, filtered through a 0.45 μm cut off membrane, concentrated 10 times with a 30 kDa cut off membrane, aliquoted and stored at −80°C.

Pseudovirus neutralization

HEK293-hACE2 cells (Crawford et al., 2020) were cultured in DMEM with 10% FBS (Hyclone) and 1% PenStrep with 8% CO_2 in a 37°C incubator (ThermoFisher). One day prior to infection, 40 μL of poly-lysine (Sigma) was placed into 96-well plates and incubated with rotation for 5 min. Poly-lysine was removed, plates were dried for 5 min then washed 1 × with water prior to plating with 40,000

cells. The following day, cells were checked to be at 80% confluence. In an empty half-area 96-well plate a 1:3 serial dilution of sera was made in DMEM and diluted pseudovirus was then added to the serial dilution and incubated at room temperature for 30-60 min. After incubation, the sera-virus mixture was added to the cells at 37°C and 2 hours post-infection, 40 μL 20% FBS-2% PenStrep DMEM was added. After 17-20 hours (VSV) or 48 hours (HIV, MLV) 40 μL/well of One-Glo-EX substrate (Promega) was added to the cells and incubated in the dark for 5-10 min prior reading on a BioTek plate reader. Measurements were done in at least duplicate. Relative luciferase units were plotted and normalized in Prism (GraphPad). Nonlinear regression of log(inhibitor) versus normalized response was used to determine IC_{50} values from curve fits. Kruskal Wallis tests were used to compare two groups to determine whether they were statistically different.

Sarbecovirus biolayer interferometry binding analysis

Purification of Fabs from NHP serum was adapted from Boyoglu-Barnum et al. (2021). Briefly, 1 mL of day 70 serum was diluted to 10 mL with PBS and incubated with 1 mL of 3 × PBS-washed protein A beads (GenScript) with agitation overnight at 37°C. The next day beads were thoroughly washed with PBS using a gravity flow column and bound Abs were eluted with 0.1 M glycine pH 3.5 into 1M Tris-HCl (pH 8.0) to a final concentration of 100 mM. Serum and early washes that flowed through were re-bound to beads overnight again for a second, repeat elution. IgGs were concentrated (Amicon 30 kDa) and buffer exchanged into PBS. 2 × digestion buffer (40 mM sodium phosphate pH 6.5, 20 mM EDTA, 40 mM cysteine) was added to concentrated and pooled IgGs. 500 μL of resuspended immobilized papain resin (ThermoFisher Scientific) freshly washed in 1 × digestion buffer (20 mM sodium phosphate, 10 mM EDTA, 20 mM cysteine, pH 6.5) was added to purified IgGs in 2 × digestion buffer and samples were agitated for 5 h at 37°C. The supernatant was separated from resin and resin washes were collected and pooled with the resin flow through. Pooled supernatants were sterile-filtered at 0.22 μm and applied 6 × to PBS-washed protein A beads in a gravity flow column. The column was eluted as described above and the papain procedure repeated overnight with undigested IgGs to increase yield. The protein A flow throughs were pooled, concentrated (using an Amicon 10 kDa), and buffer exchanged into PBS. Purity was checked by SDS-PAGE.

Assays were performed and analyzed using biolayer interferometry on an Octet Red 96 System (Pall Forte Bio/Sartorius) at ambient temperature with shaking at 1000 rpm. Different Sarbeco RBDs were purified like in Walls et al., 2020 and were diluted with different acetate buffers and applied to a black 96-well Greiner Bio-one microplate at 200ul per well. GD-Pangolin RBD was diluted in pH 6 buffer to 5 μg/mL, RmNY02 were diluted in pH 5 to 25 μg/mL, WIV16 was diluted in pH 5 to 10 μg/mL, SARS-CoV-2 was diluted in pH 6 to 5 μg/mL, RaTG13 was diluted in pH 6 to 10 μg/mL, RaTG13 was diluted in pH 6 to 10 μg/mL, SARS-CoV was diluted in pH 6 to 50 μg/mL, and finally ZXC21 was diluted in pH 6 to 10μg/mL. AR2G biosensors (ForteBio/Sartorius) following 600 s hydration were normalized in water for 180 s. Then tips were NHS-EDC activated for 300 s and the different sarbecovirus RBDs were loaded up to a 1.50 nm threshold for up to 600 s. Immobilized RBDs on the tips were quenched for 300 s in ethanolamine and dipped into kinetics buffer for a 60 s baseline. The association step was performed by dipping the mobilized RBDs into diluted purified polyclonal pigtail macaque IgGs for 600 s. Dissociation was measured by inserting the biosensors in kinetics buffer for 600 s. The data were baseline subtracted and the plots fitted using the Pall ForteBio/Sartorius analysis software (version 12.0).

Cocktail and mosaic bio-layer interferometry (antigenicity)

Binding of hACE2-Fc to monovalent RBD-I53-50 nanoparticles, mosaic-RBD-I53-50 nanoparticles, and cocktail of RBD-nanoparticles was analyzed for antigenicity experiments and real-time stability studies using an Octet Red 96 System (Pall FortéBio/Sartorius) at ambient temperature with shaking at 1000 rpm. Protein samples were diluted to 100 nM in Kinetics buffer (1 × HEPES-EP+ (Pall Forté Bio), 0.05% nonfat milk, and 0.02% sodium azide). Buffer, receptor, and analyte were then applied to a black 96-well Greiner Bio-one microplate at 200 μL per well. Protein A biosensors (FortéBio/Sartorius) were first hydrated for 10 minutes in Kinetics buffer, then dipped into hACE2-Fc diluted to 10 μg/mL in Kinetics buffer in the immobilization step. After 150 s, the tips were transferred to kinetics buffer for 60 s to reach a baseline. The association step was performed by dipping the loaded biosensors into the immunogens for 300 s, and subsequent dissociation was performed by dipping the biosensors back into Kinetics buffer for an additional 300 s. The data were baseline subtracted prior for plotting using the FortéBio analysis software (version 12.0). Plots in Figure S3 show the 600 s of association and dissociation.

Sandwich bio-layer interferometry (mosaic display antigenicity)

Binding of hACE2-Fc or S2H14 mAb and S230 Fab to WIV1-RBD-I53-50, RaTG13-RBD-I53-50, SARS-CoV-SARS-CoV2-RBD-I53-50, SARS-CoV2-I53-50, and mosaic-RBD-I53-50 nanoparticles were analyzed for co-display of RBDs using an Octet Red 96 System (Pall FortéBio/Sartorius) at ambient temperature with shaking at 1000 rpm. Nanoparticles were diluted to 100 nM in Kinetics buffer. Kinetics buffer, mAb, nanoparticles and Fab were then applied to a black 96-well Greiner Bio-one microplate at 200 μL per well. Protein A biosensors (FortéBio/Sartorius) were first hydrated for 10 minutes in Kinetics buffer, then dipped into hACE2-Fc or S2H14 mAb diluted to 10 μg/mL in Kinetics buffer in the immobilization step. After 150 s, the tips were transferred to Kinetics buffer for 60 s to reach a baseline. The receptor or mAb was then loaded with nanoparticle by dipping the loaded biosensors into the immunogens for 300 s, and subsequent baseline was performed by dipping the biosensors back into the Kinetics buffer for an additional 60 s. Association of S230 Fab diluted to 100 nM in Kinetics buffer was then measured for 300 s and subsequent dissociation in Kinetics buffer of S230 Fab for 300 s. The data were baseline subtracted prior for plotting using the FortéBio analysis software (version 12.0). Plots in Figure S3 exclude the initial mAb loading and the first baseline.

Cocktail and mosaic negative stain electron microscopy

Monovalent RBD-I53-50 nanoparticles, mosaic-RBD-I53-50 nanoparticles, and cocktail of RBD-nanoparticles were first diluted to 75 μg/mL in 50 mM Tris pH 7.4, 185 mM NaCl, 100 mM Arginine, 4.5% v/v Glycerol, 0.75% w/v CHAPS prior to application of 3 μL of sample onto freshly glow-discharged 300-mesh copper grids. Sample was incubated on the grid for 1 minute before the grid was dipped in a 50 μL droplet of water and excess liquid blotted away with filter paper (Whatman). The grids were then dipped into 6 μL of 0.75% w/v uranyl formate stain. Stain was blotted off with filter paper, then the grids were dipped into another 6 μL of stain and incubated for ~70 s. Finally, the stain was blotted away and the grids were allowed to dry for 1 minute. Prepared grids were imaged in a Talos model L120C electron microscope at 57,000 × (nanoparticles).

Cocktail and mosaic dynamic light scattering

Dynamic Light Scattering (DLS) was used to measure hydrodynamic diameter (Dh) and % Polydispersity (%Pd) of monovalent RBD-I53-50 nanoparticles, mosaic-RBD-I53-50 nanoparticles, and cocktail of RBD-nanoparticles on an UNcle Nano-DSF (UNchained Laboratories). Sample was applied to a 8.8 μL quartz capillary cassette (UNi, UNchained Laboratories) and measured with 10 acquisitions of 5 s each, using auto-attenuation of the laser. Increased viscosity due to 4.5% v/v glycerol in the RBD nanoparticle buffer was accounted for by the UNcle Client software in Dh measurements.

Mouse immunizations and challenge

At six weeks of age, 8 female BALB/c mice per dosing group were vaccinated with a prime immunization, and three weeks later mice were boosted with a second vaccination (IACUC protocol 4470.01). Prior to inoculation, immunogen suspensions were gently mixed 1:1 vol/vol with AddaVax adjuvant (Invivogen, San Diego, CA) to reach a final concentration of 0.01 mg/mL antigen. Mice were injected intramuscularly into the gastrocnemius muscle of each hind leg using a 27-gauge needle (BD, San Diego, CA) with 50 μL per injection site (100 μL total) of immunogen under isoflurane anesthesia. To obtain sera all mice were bled two weeks after prime and boost immunizations. Blood was collected via submental venous puncture and rested in 1.5 mL plastic Eppendorf tubes at room temperature for 30 min to allow for coagulation. Serum was separated from red blood cells via centrifugation at 2,000 g for 10 min. Complement factors and pathogens in isolated serum were heat-inactivated via incubation at 56°C for 60 min. Serum was stored at 4°C or −80°C until use. The study was repeated twice. Five weeks post-boost, mice (aged 14 weeks) were exported from Comparative Medicine Facility at the University of Washington, Seattle, WA to an AAALAC accredited Animal Biosafety Level 3 (ABSL3) Laboratory at the University of North Carolina, Chapel Hill. After a 7-day acclimation time, mice were anesthetized with a mixture of ketamine/xylazine and challenged intranasally with 10^5 plaque-forming units (pfu) of mouse-adapted SARS-CoV-2 MA10 or SARS-CoV MA15 strain for the evaluation of vaccine efficacy (IACUC protocol 20-114.0). After infection, body weight and congestion score were monitored daily until the termination of the study two days post-infection, when lung and nasal turbinate tissues were harvested to evaluate viral load by plaque assay.

Histopathology of post challenge mouse lungs

For each mouse the left lung was incubated in formalin at 4°C for at least 7 days to fix tissue and inactivate virus. The fixed tissue was processed and embedded in paraffin. 5 μm sections were cut and stained with either Congo red or hematoxylin and eosin (H&E). Eosinophils were enumerated by counting the Congo red positive leukocytes in 10 high power fields (400X final magnification) per mouse lung. Representative images were minimally and similarly adjusted with Adobe Photoshop 2020 to enhance contrast. Airway pathology was assessed in H&E stained sections to assess bronchial epithelial cell death (score: 0 = no dead cells, 1 = 1-5 dead cells, 2 = 6-10 dead cells, 3 = 11-20 dead cells and 4 = > 20 dead cells; scored for 10 400X fields per mouse lung), peribronchial inflammation (score 0 = none, 1 = 0%–25% circumference with > 1 leukocyte cell layer, 2 = 26%–50% circumference with > 1 leukocyte cell layer, and 3 = 50%–100% circumference with > 1 leukocyte cell layer; scored for 10 400X fields per mouse lung), and interstitial pneumonitis (score = percentage of pulmonary alveolar parenchyma with septae expanded by leukocyte; scored for 10 100X fields).

QUANTIFICATION AND STATISTICAL ANALYSIS

Statistical details of experiments can be found in the figure legends. For NHP experiments, 2-6 sera samples were used and experiments were done in at least duplicate unless mentioned. For mouse ELISAs, neutralization, and challenge experiments, sera from 6, 8, or 10 BALB/c animals were used and experiments were completed in at least duplicate unless mentioned. Geometric mean titers were calculated. Kruskal Wallis tests were performed to compare two groups to determine whether they were statistically different for ELISA and neutralization experiments. Significance is indicated with stars: *, $p < 0.05$; **** $p < 0.0001$ and non significant groups are not shown.

Supplemental figures

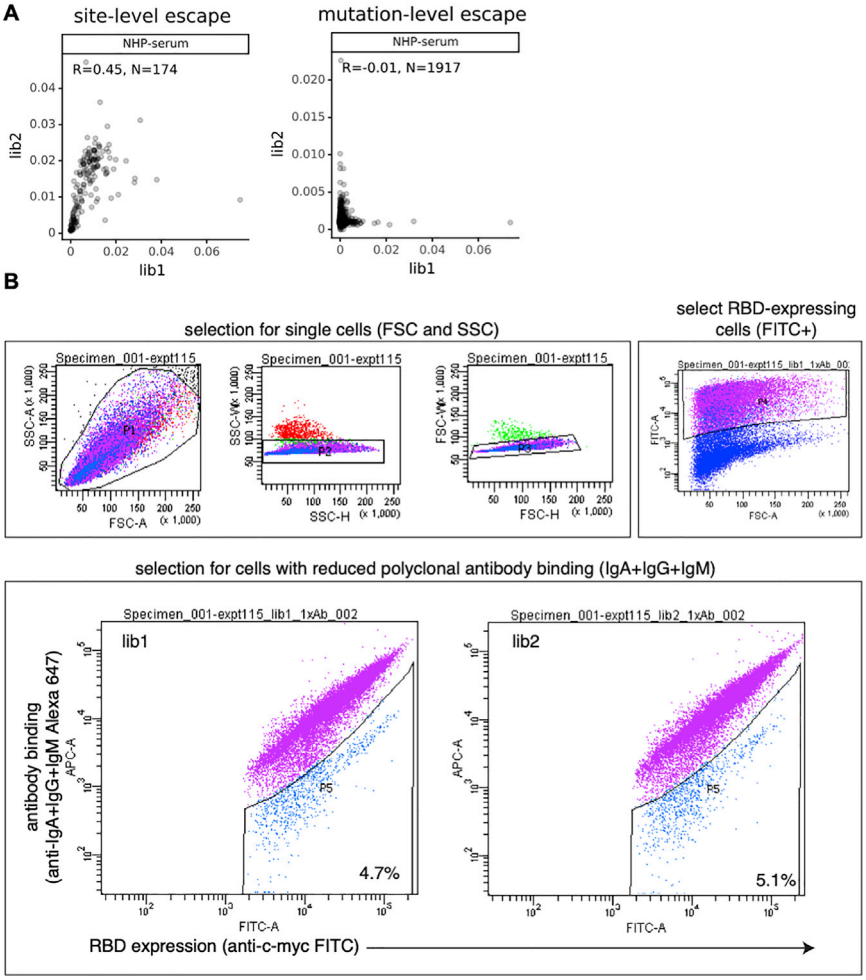

Figure S1. Effects of mutations on binding of HCP Abs to RBD and FACS gating strategy, related to Figure 2

(A) Correlation plots of site- and mutation-level escape for each of the two independent RBD mutant libraries for the Ab-escape map shown in Figure 2B. Site-level escape is the sum of the escape fractions for each mutation at a site. (B) Hierarchical FACS gating strategy used for selecting yeast cells expressing Ab-escape RBD variants. First, gates are selected to enrich for single cells (SSC-A versus FSC-A, and FSC-W versus FSC-H) that also express RBD (FITC-A versus FSC-A, cells in pink). Second, cells expressing RBD mutants with reduced polyclonal Ab binding, detected with an anti-IgA+IgG+IgM secondary Ab, were selected with a gate that captured the ~5% of cells with the lowest Ab binding (cells in blue).

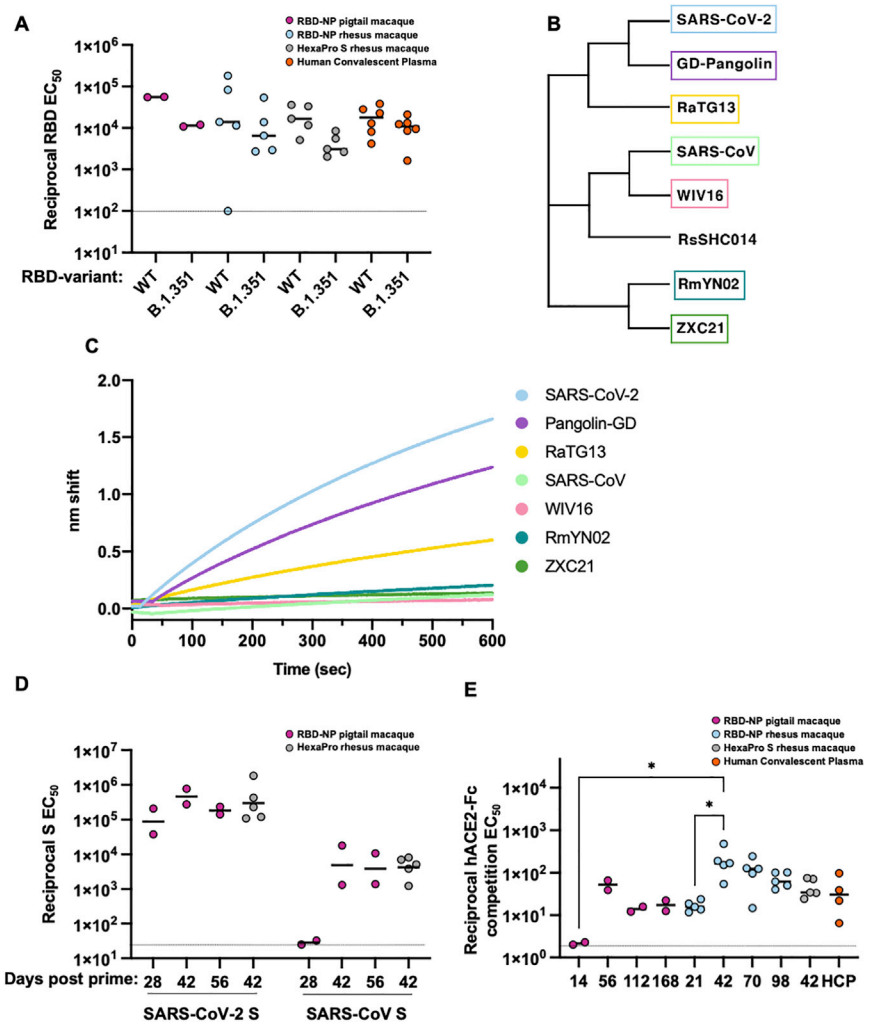

Figure S2. Evaluation of vaccine-elicited binding and neutralizing Ab titers against SARS-CoV-2 variants and sarbecoviruses, related to Figure 3

(A) Wild-type (Wuhan-Hu-1) and B.1.351 SARS-CoV-2 RBD-specific Ab binding titers of RBD-NP-elicited sera in pigtail macaques (magenta, n = 2) and rhesus macaques (blue, n = 5), HexaPro S-elicited sera in rhesus macaques (gray, n = 5), or HCP (orange, n = 6, Table S1) analyzed by ELISA with an LOD of $1x10^2$. (B) Cladogram based on sarbecovirus RBD amino acid sequences. (C) Biolayer interferometry analysis of binding of 1 μM purified polyclonal pigtail macaque IgGs (obtained 70 days post prime) to sarbecovirus RBDs immobilized at the surface of biosensors. (D) SARS-CoV-2 S2P (left) or SARS-CoV S2P (right) Ab binding titers of RBD-NP-elicited sera in pigtail macaques (magenta) or HexaPro S-elicited sera in rhesus macaques (gray) analyzed by ELISA with an LOD of 2.5×10^1. (E) Competition ELISA between 0.13 nM human ACE2-Fc and RBD-NP-elicited sera in pigtail macaques (magenta) and rhesus macaques (blue), or HexaPro S-elicited sera in rhesus macaques (gray) at various time points following vaccination, benchmarked against COVID-19 HCP with an LOD of $4 \times 10^{\circ}$, showing the magnitude of inhibition of ACE2 binding to immobilized SARS-CoV S2P expressed as reciprocal serum dilution blocking 50% of the maximum binding response. Statistical significance was determined by Kruskal-Wallis test and shown when significant. **, $p < 0.01$. All data repeated twice. LODs are shown as gray horizontal dotted lines. Raw data curves shown in Data S1.

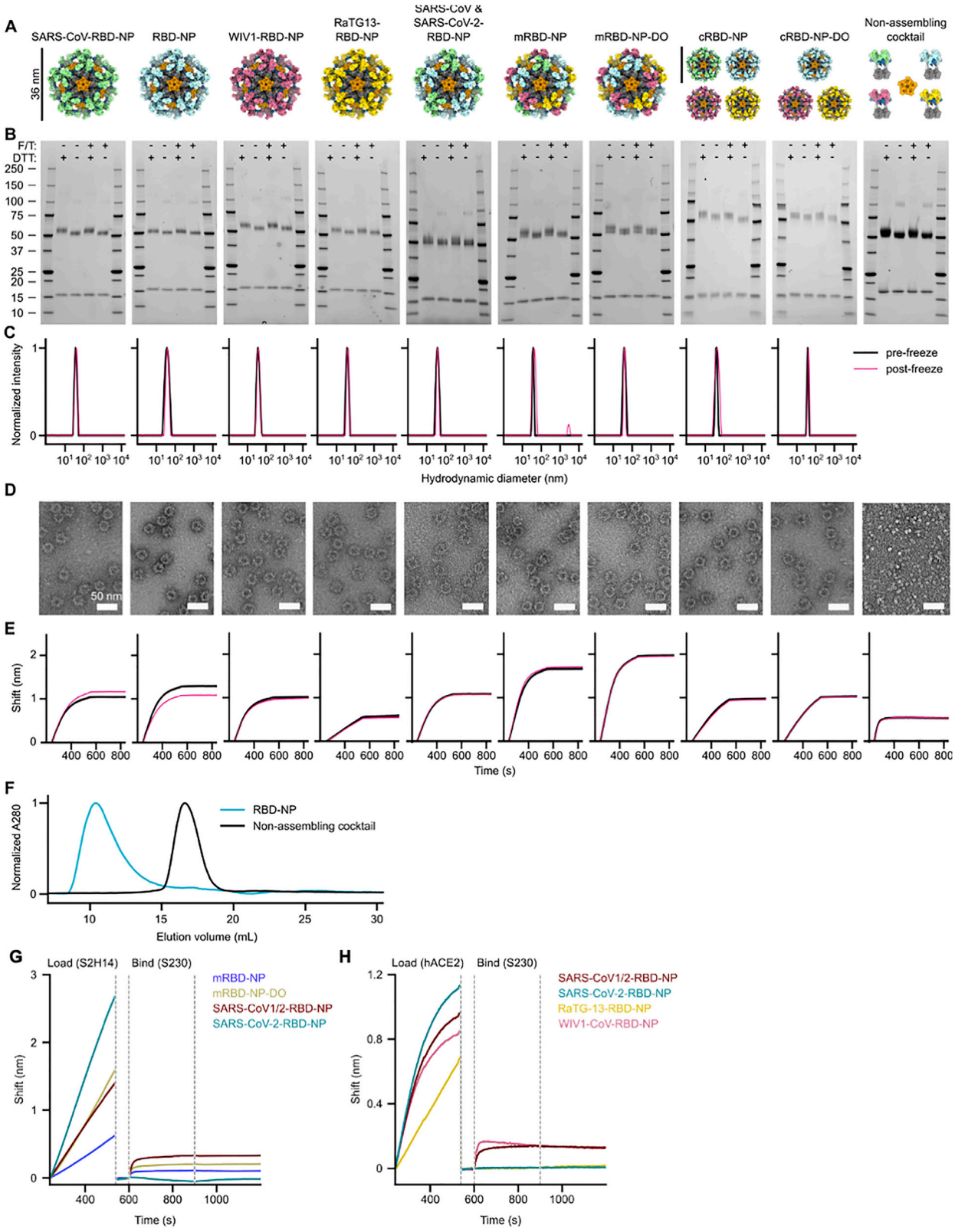

(legend on next page)

Figure S3. *In vitro* characterization and confirmation of co-display of sarbecovirus RBD-NP immunogens, related to Figure 4

(A) Design models of the various vaccine candidates evaluated. Scale bars, 36 nm. (B) SDS-PAGE analysis of purified nanoparticles. DTT, dithiothreitol; F/T, freeze/thaw. (C) Dynamic light scattering. (D) Electron micrographs of negatively stained samples. Scale bars, 50 nm. (E) Binding of 100 nM SEC-purified nanoparticle immunogens and the non-assembling cocktail immunogen (which was not purified with SEC) to immobilized hACE2-Fc. (F) SEC chromatogram overlay of purified RBD-NP and non-assembling cocktail. (G-H) Sandwich biolayer interferometry. The SARS-CoV-2 S-specific mAb S2H14 immobilized on protein A biosensors was used to capture various nanoparticle immunogens from 300-480 s. The captured nanoparticles were subsequently exposed to a Fab derived from the SARS-CoV S-specific mAb S230 from 600-900 s (G). hACE2-Fc immobilized on protein A biosensors was used to capture various nanoparticle immunogens from 300-480 s. The captured nanoparticles were subsequently exposed to a Fab derived from the SARS-CoV S-specific mAb S230 from 600-900 s (H).

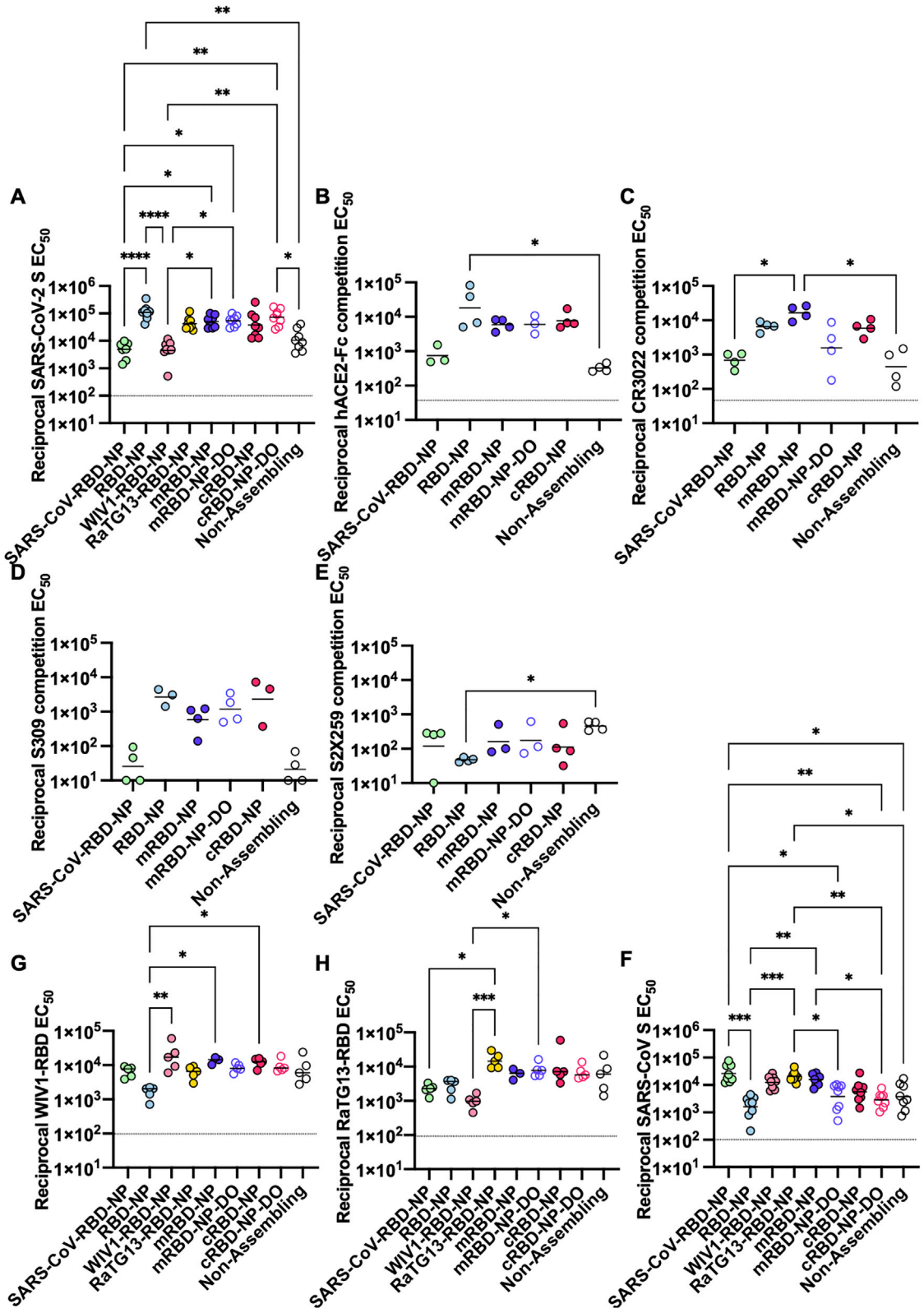

(legend on next page)

Figure S4. Serum Ab binding titers elicited by mosaic and cocktail RBD-NPs, related to Figure 5

(A) Ab binding titers to SARS-CoV-2 S2P at five weeks post prime analyzed by ELISA with an LOD of $1x10^2$. (B–E) Titers of SARS-CoV-2 S-specific Abs competing with ACE2-Fc with an LOD of $5x10^1$ (B), CR3022 with an LOD of $5x10^1$ (C), S309 with an LOD of $1x10^1$ (D), and S2X259 with an LOD of $1x10^1$ (E) in immunized mouse sera analyzed by competition ELISA. (F) Ab binding titers to SARS-CoV S2P at week 5 analyzed by ELISA. (G–H) Ab binding titers to the WIV1 (G), and RaTG13 (H) RBDs analyzed by ELISA with an LOD of $1x10^2$. Statistical significance was determined by Kruskal Wallis test and shown when significant. $^{**}p < 0.01$. LODs are shown as gray horizontal dotted lines. Raw data curves shown in Data S1.

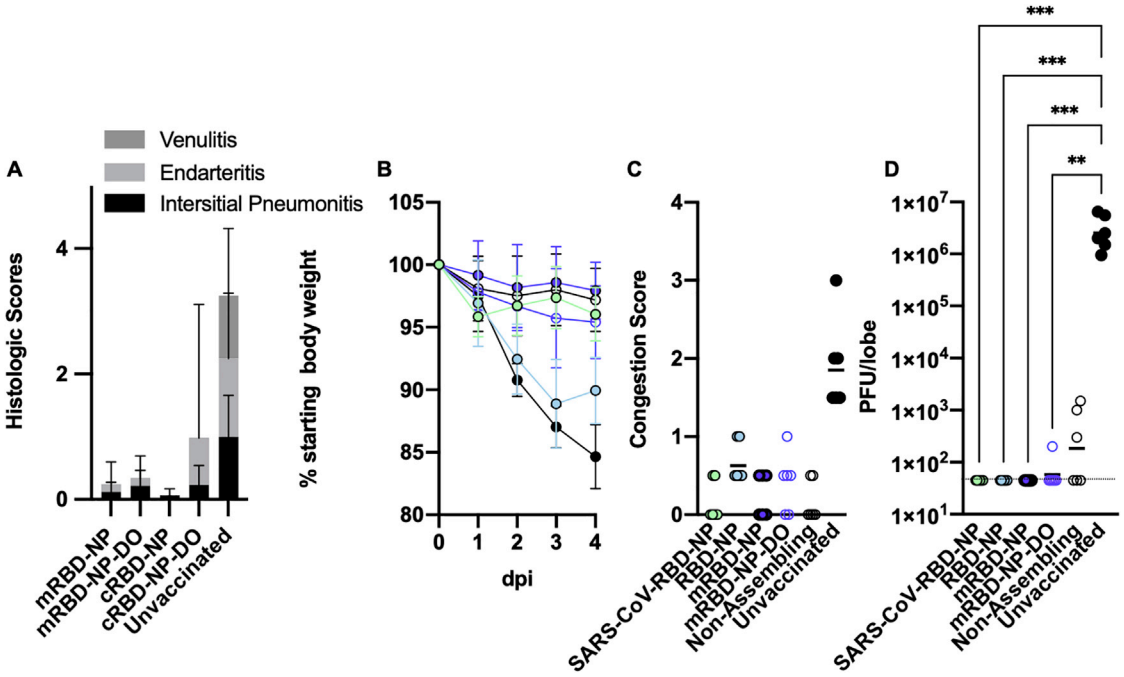

Figure S5. Monovalent, mosaic, and cocktail RBD-NPs protect against heterotypic SARS-CoV-MA15 challenge in 15-week-old BALB/c cByJ mice, related to Figure 6

(A) Normalized active inflammation following SARS-CoV MA 15 challenge shown in Figure 6 with venulitis, endarteritis, and interstitial pneumonitis shown as stacked bar graphs in dark gray, light gray, and black respectively. (B) Weight loss following SARS-CoV MA15 challenge (N = 6). Unvaccinated animals are shown as black circles. (C) Congestion score following SARS-CoV MA15 challenge with a score of 0 indicating unchanged lung color and 4 indicating a darkened and diseased lung (N = 6). (D) Viral titers in mice lungs (expressed in plaque forming units per lobe) following challenge (N = 8) with an LOD of $9x10^1$. Statistical significance was determined by Kruskal Wallis test and shown when significant and $^{**}p < 0.01$. LOD is shown as a gray horizontal dotted line.